COMPDYN 2013
4th ECCOMAS Thematic Conference on
Computational Methods in Structural Dynamics and Earthquake Engineering
M. Papadrakakis, V. Papadopoulos, V. Plevris (eds.)
Kos Island, Greece, 12–14 June 2013

RAPID EVALUATION OF NON-DUCTILE MULTISTOREY RC BUILDINGS

Georgia E. Thermou[1] **and Anastasia F. Palaiochorinou**[1]

[1] Aristotle University of Thessaloniki
Dept. of Civil Engineering, 54124, Thessaloniki, Greece
gthermou@civil.auth.gr; palaiochorinou@teeemail.gr

Keywords: Assessment, Gravity Load bearing buildings, Prioritizing of Failure Modes, Collapse, Reinforced Concrete.

Abstract. *The majority of existing building stock in southern Europe, as well as in other parts of the world, comprises non-ductile multistory reinforced concrete (RC) buildings designed for gravity loads only without any reinforcement detailing. The deficiencies of such structures lead to premature failure or collapse, posing a realistic threat to human life. Thus, assessment of their seismic vulnerability is deemed necessary, by examining in detail their response to various scenarios. Due to the large inventory of this type of buildings such an effort requires huge amounts of work, rendering the whole procedure unrealistic. For this purpose a rapid preliminary assessment methodology was proposed by Thermou and Pantazopoulou [1], Pardalopoulos et al. [2], which aims to single out those buildings that are at a greater risk for catastrophic collapse and in which further detailed assessment with the aid of advanced analytical tools is deemed necessary. The methodology is based on the stiffness index (used to determine the severity of seismic displacement demand) and the base-shear strength index (associated with typical column details representative of the state of practice from the era of the building's period of construction) criteria.*

Within the framework of current research, a database of ten representative multistory RC residential buildings that were built in the 1950's in Northern Greece (in the city of Thessaloniki) was created. This group of buildings was assessed by using the aforementioned rapid preliminary assessment methodology for various scenarios related to increasing peak ground acceleration (PGA) values. The characteristics of this prevalent construction type were recorded after extensive study of the design drawings of real structures of the era and are presented herein.

An eight-storey RC building was selected from the database for detailed implementation of the proposed rapid assessment methodology throughout its storeys. The validity of the preliminary assessment methodology was verified by conducting numerous detailed analyses. For this purpose, a three-dimensional finite element model was created and pushover analyses were carried out. The influence of the masonry infills was another parameter of study. The results verified the outcome of the rapid evaluation methodology and complied with the findings of the reconnaissance report.

1 INTRODUCTION

The design philosophy of buildings in earthquake prone areas has changed dramatically the last thirty years given the experience gained from major earthquake events which revealed the susceptibility of older construction units. It is a fact that the majority of multi-storey reinforced concrete (RC) buildings in southern Europe was designed according to older generation of codes where reinforcement detailing was at a primitive stage of knowledge. The deficiencies of such structures lead to premature failure or collapse, posing a realistic threat to human life. Recent earthquakes underlined the need for assessment of their seismic vulnerability. Considering the large inventory of this type of buildings analytical modeling requires huge amounts of work, rendering the whole procedure unrealistic. Therefore rapid and palatable tools for assessing the seismic vulnerability of the built environment need be developed. Within this context, a rapid preliminary assessment methodology was proposed by Thermou and Pantazopoulou [1], Pardalopoulos et al. [2], which aims to single out those buildings that are at a greater risk for catastrophic collapse and in which further detailed assessment with the aid of advanced analytical tools is deemed necessary.

One of the objectives of this paper is to shed light on the response of multistory RC residential buildings that were built in the 1950's in the city of Thessaloniki (Greece). Given that the first Greek Seismic Code was launched in 1959 and that RC walls were introduced in construction in the 1960's, multistory buildings of the '50's represent the cutting edge of the construction technology for gravity load designed frame buildings. A database of ten representative multistory RC residential buildings that were built in the 1950's in the city of Thessaloniki (in Northern Greece) was created. The characteristics of this prevalent construction type were recorded after extensive study of the design drawings of real structures of the era and are presented herein. Despite the fact that gravity load design principles were implemented, this type of building units survived the 1978 Thessaloniki earthquake (PGA=0.15g) with moderate or no damage at all.

The proposed preliminary assessment methodology was applied to one representative eight-storey RC building selected from the database. A common feature of this type of buildings is the change of column dimensions and longitudinal reinforcement from storey to storey. This implies that the methodology needs to be applied in each storey and that the critical storey cannot be defined a priori. The primary deficiencies of the building and the level of spectral acceleration that may be tolerated prior to failure were defined after implementation of the stiffness and strength criteria.

The validity of the rapid evaluation methodology was verified by conducting detailed pushover analyses. For this purpose, a finite element program was utilized where modeling required the determination of the nonlinear properties of each component in the structure, quantified by strength and deformation capacities. With parameters of study the existence or no of external infill walls throughout the structure, the type of the plastic hinges (automatic or user-defined hinges, shear hinges) a group of three-dimensional models was created and pushover analysis were carried out. The results verified the outcome of the rapid evaluation methodology and complied with the findings of the reconnaissance report.

2 CHARACTERISTICS OF THE GRAVITY LOAD DESIGNED RC BUILDINGS

A group of ten multistory representative RC residential buildings that were built in the 1950's in the city of Thessaloniki (Greece) comprises the database created for the needs of current research. A common feature of this type of building unit refers to the open first storey

for store or parking lot usage, known as *pilotis* (Fig.1), and the existence of penthouses introducing in-height irregularities of mass and stiffness distribution.

Given that the first Greek Seismic Code was launched in 1959, the gravity load design principles were followed in the 1950's buildings. The allowable stress design philosophy was implemented not allowing any control of the mode of failure and the corresponding deformation capacity of the individual members. Reinforcement detailing followed empirical rules of the era, rarely specified in official drawings. This was confirmed after studying the folders of numerous buildings of this era. One of the criteria followed for ending up to the ten representative buildings was the level of completeness of the folders. The information gathered and presented in the following two paragraphs refers to the material characteristics, construction detailing and geometrical configuration characteristics.

Figure 1: Typical multistory RC residential buildings with pilotis in Greece.

The materials used in the 1950's are characterized by low strength and lack of quality control. Concrete was constructed at site with the use of a concrete mixer machine and was carried by the workers. In case of steel, metallurgical testing was at a primitive stage and credentials were never questioned. Another parameter that influences greatly the quality of construction is supervision which was relatively lenient, thus rendering the experience of the workers a determinant factor for the quality of construction.

The concrete qualities used according to the Greek Royal Decree No.18.2/1954 [3] were the B120 and the B160 with a characteristic cylindrical strength equal to $f_{ck}\cong 8$ MPa and $f_{ck}\cong 10$ MPa. Smooth steel reinforcing bars were used of quality StI with a characteristic yield strength $f_{yk}=220$ MPa ([4]).

As far as construction practice is concerned, longitudinal reinforcement bars of 10 mm – 20 mm diameter and 6 mm – 8 mm diameter stirrups spaced at 200 mm – 600 mm were applied in both columns and beams. Stirrups in both columns' and beams' sections were anchored with 90° hooks in the ends (open stirrups). Lap splices were usually unconfined, whereas starter bars had random lengths. Joints were usually left without stirrups, for convenience of construction. Longitudinal reinforcement with hooks were used with arbitrary lengths not specified in the official drawings. Often in-plan column layout is not on grid leading to indirect supports (i.e. primary beam supporting secondary).

The buildings of the 1950's are characterized as frame buildings having usually up to three spans. The lack of a continuous vertical load path along the height of the buildings is a common feature of the buildings of that era. Symmetry in columns' layout along one or two axes in some cases is observed. Note that RC walls do not exist in the stuctures of the era

neither as an additional load bearing system nor in the stairwells or in the elevator shafts since their implementetaion was introduced in the early 1960's in Greece. Typical columns' cross section dimensions ranged between 300 mm – 600 mm decreasing in the upper floors. Their longitudinal reinforcement ratio ranged between 7‰ - 9‰ lower than the minimum reinforcement defined by the modern codes equal to 10‰ [6]. Referring to beams their typical cross section dimensions were 150 mm × 300 mm to 300 mm × 600 mm. Slab thickness ranged between 100 mm – 120 mm. The findings of real structures construction practice research are summarised in Table 1.

Construction practice characteristics	
Concrete quality	B120 ÷ B160 $^{(*)}$ (f_{ck}≅8-10 MPa)
Steel quality (longitudinal and transverse reinforcement)	Smooth StI (f_{yk}=220 MPa) $^{(**)}$
Typical columns' cross section dimensions	300 ÷ 600 mm
Typical diameters of columns' longitudinal reinforcement bars	Ø14 ÷ Ø20
Typical columns' transverse reinforcement	Ø6/250 ÷ 300 mm $^{(***)}$
Typical columns' longitudinal reinforcement ratio	7‰ ÷ 9‰ < 10‰
Typical beams' cross section dimensions	150×300 ÷ 300×600 mm
Typical diameters of beams' longitudinal reinforcement bars	Ø10 ÷ Ø18
Typical beams' transverse reinforcement	Ø6/200 ÷ 250 mm $^{(***)}$
Typical thickness of masonry infill walls	100 mm for internal 200 mm for external
Anchorage / lap splices construction practice	• Longitudinal reinforcement with hooks with arbitrary lengths. • Stirrups anchored with 90° hooks. • Unconfined lap splices.

$^{(*)}$ as per Greek Royal Decree No.18.2/1954 [3]. Later concrete quality B225 (f_{ck}≅14MPa) was introduced in construction, $^{(**)}$ as per DIN 1045 (1936) [4]. Later longitudinal reinforcement steel quality was differentiated to StIII (f_{yk}=400÷420MPa), $^{(***)}$ rarely diameter Ø8 was applied.

Table 1: Information of the typical construction practice followed in the early 1950's in Greece.

3 RAPID EVALUATION METHODOLOGY

Preliminary assessment of existing building stock targeted toward identification of the most vulnerable buildings must necessarily rely on a marginal collection of data that is readily available, such as the overall geometric details of the structure (number of floors, floor height, floor area, location and gross geometry of load carrying members in plan), on the implicit assumption that all reinforcing details are represented by the historical construction information for the period and region of construction of the building studied.

The rapid preliminary seismic vulnerability assessment methodology is based on the:

(a) Stiffness criterion, which is used to quantify interstorey drift demand and thus evaluate the severity of seismic displacement demand.

(b) Strength criterion, which is used to determine the weakest mechanism of resistance, likely to control the sequence of failure of the vertical elements of the structure.

3.1 Estimation of storey stiffness

The stiffness K_i of the i-th storey of a frame building that comprises columns (K_i^c) and masonry infill walls stiffnesses (K_i^{wm}) is given by [1]:

$$K_i = K_i^c + K_i^{wm} = \frac{A_f}{h_i}\left(D_c\rho_{c,i} + D_{wm}\rho_{wm,i}\right) = \frac{A_f}{h_i} D_c\rho_i^e \tag{1}$$

$$\text{with } D_c = E_c\left(\frac{h_{c,ave}}{h_i}\right)^2,\ D_{wm} = 0.10\frac{f_{bc}^{0.7} f_{mc}^{0.3}}{\mu_y^{wm}\theta_y^{wm}} \text{ and } \rho_i^e = \rho_{c,i}\left(1 + \frac{D_{wm}}{D_c}\frac{\rho_{wm,i}}{\rho_{c,i}}\right)$$

where A_f (m^2) is the i-th floor area, h_i (m) is the clear i-th storey height, $E_c=22\ (f_{ck}/10)^{1/3}$ (GPa) is the concrete modulus of elasticity [6], $h_{c,ave}$ (m) the average column cross section height, $\rho_{c,i}$ the dimensionless area ratio of columns at the i-th floor plan, $\rho_{wm,i}$ the dimensionless area ratio of masonry walls at the i-th floor plan, ρ_i^e is the equivalent dimensionless area ratio of vertical members at the i-th floor plan, f_{bc} (MPa) is the bricks compressive strength, f_{mc} (MPa) mortar compressive strength, μ_y^{wm} the drift ductility of masonry walls and θ_y^{wm} the drift of masonry walls at yield.

3.2 Interstorey Drift Spectra (IDS) for frame buildings

Interstorey Drift Spectra (IDS) was developed by Thermou et al. [5] as an efficient tool for the seismic upgrading of existing RC buildings. In this type of spectra, stiffness demand is related to the target response of the building. For the needs of assessment, stiffness demand is expressed as a function of the equivalent dimensionless area ratio of vertical members, whereas interstorey drift is considered a measure of the system's vulnerability and [1]. The methodology of derivation of the IDS for the i-th storey follows.

Type I elastic spectrum of Eurocode 8 [7] is used to define spectral displacement demand for a design region $0.15s < T < 2.00\ s$ for subsoil class B with S=1.20, β_0=2.50, T_B=0.15 s, T_C=0.50 s, q=1.00, as follows:

$$0.15 \le T \le 0.50:\ S_d(T) = 0.076\alpha_g T^2 \tag{2a}$$

$$0.50 < T \le 2.00:\ S_d(T) = 0.038\alpha_g T \tag{2b}$$

where a_g is the peak ground acceleration (pga), β_o is spectral acceleration amplification factor equal to 2.5, S is the soil parameter, and T_B, T_C are the period values that define the limits of the constant acceleration branch.

Period T of an n-storey building with constant distribution of storey stiffness and storey plan geometry along the height of the building is given by:

$$T = 2\pi/\omega = 2\left(2n+1\right)\sqrt{M_i/K_i} = 2\left(2n+1\right)\left(\frac{\gamma h_i}{D_c\rho_i^e}\right)^{0.5} \tag{3}$$

where n is the number of storeys, M_i is the storey mass, K_i is the storey stiffness (Eq. (1)), $\gamma(=M_i/A_f)$ is the mass per unit area of the floor, h_i is the i-th storey height, D_c is defined in Eq. (1) and ρ_i^e is the equivalent dimensionless area ratio of vertical members at the i-th floor plan.

The substitution of T in Eqs. (2) relates the spectral displacement demand with the equivalent dimensionless area ratio of vertical members at the i-th floor plan as follows:

$$0.15 \le T \le 0.50: \; S_d(T) = 0.304\alpha_g \left(2n+1\right)^2 \left(\frac{\gamma h_i}{D_c \rho_i^e}\right) \tag{4a}$$

$$0.50 < T \le 2.00: S_d(T) = 0.076\alpha_g \left(2n+1\right)\left(\frac{\gamma h_i}{D_c \rho_i^e}\right)^{0.5} \tag{4b}$$

where a_g is the peak ground acceleration (pga), n is the number of storeys, $\gamma(=M_i/h_i)$ is the mass per unit area of the floor, h_i is the i-th storey height, D_c is defined in Eq. (1) and ρ_i^e is the equivalent dimensionless area ratio of vertical members at the i-th floor plan.

For frame structures the deformed shape under lateral sway may be approximated by the response shape of a shear-type building:

$$\Phi(x) = \sin\left(\frac{\pi x}{2H_{tot}}\right) \tag{5}$$

where x is the storey height from the ground level and H_{tot} is the total building height (Fig. 2).

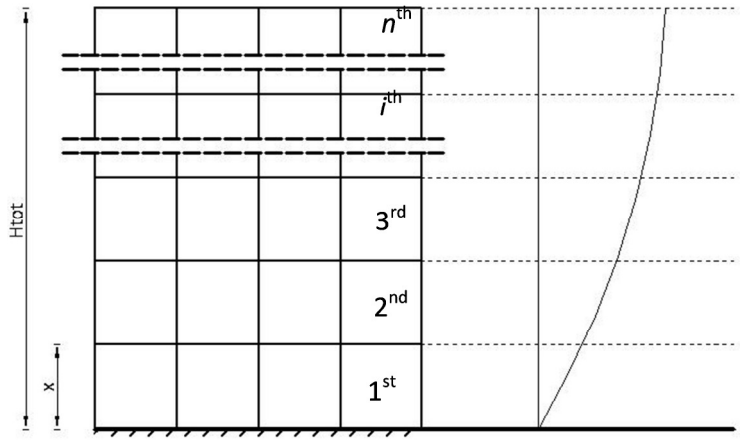

Figure 2: Lateral response shape for frame structures.

Interstorey drift of the i-th storey, Θ_i, is given by:

$$\Theta_i = S_d / h_i \Delta\Phi_i \tag{6}$$

where S_d is the spectral displacement, h_i is i-th storey height and $\Delta\Phi_i$ is the difference in the shape between successive floors.

By substituting Eqs. (4) into Eq. (6) and also by substituting the term D_c from Eq. 1, a design spectrum for the i-th interstorey drift demand under the design earthquake is extracted:

$$0.15 \le T \le 0.50: \; \Theta_i = 0.304\alpha_g \left(2n+1\right)^2 \frac{\gamma}{E_c}\left(\frac{h_i}{h_{c,ave}}\right)^2 \frac{\Delta\Phi_i}{\rho_i^e} \tag{7a}$$

$$0.50 < T \le 2.00: \; \Theta_i = 0.076\alpha_g \left(2n+1\right)\left(\frac{\gamma}{\mathrm{E}_c}\right)^{0.5} \frac{h_i^{0.5}}{h_{c,ave}} \frac{\Delta\Phi_i}{\left(\rho_i^e\right)^{0.5}} \tag{7b}$$

3.3 Estimation of storey drift at failure, $\Theta_{fail,i}$

The comparison between the interstorey drift demand, Θ_i, and drift at failure, $\Theta_{fail,i}$, provides information relative to whether the building will fail or not. In case of inadequate shear resistance collapse could be prevented if $\Theta_i<\Theta_{fail,i}$. The interstorey drift at failure, $\Theta_{fail,i}$, is estimated by considering the average interstorey drift at failure of the vertical members, $\Theta_{fail,i}^{c}$, through coefficient λ_c that expresses the relative column stiffness ratio in the frame connections of the building [1]: $\Theta_{fail,i}=\Theta_{fail,i}^{c}/\lambda_c$. The average values of λ_c estimated for the 1950's building database ranged between 0.25 ÷ 0.50.

In order to determine $\Theta_{fail,i}^{c}$ the nominal drift at yield $\Theta_{y,nom,i}^{c}$ should be calculated first and then corrected by the strength index $r_{u,lim}$, i.e. $\Theta_{fail,i}^{c} = \Theta_{y,nom,i}^{c} \cdot r_{u,lim}$ [2]. Interstorey drift at column yielding may be estimated using the 'stick model' cantilever extending from the support to the point of inflection around the midheight of the column. Thus, $\Theta_{y,nom}^{c}=1/3\ \varphi_y L_s$, where $\varphi_y = 1.77\ \varepsilon_{sy}/h_c$ [8], ε_{sy} is the steel strain at yield, h_c is the height of the cross section and L_s is the shear span length equal to the half clear storey height.

Strength index $r_{u,lim}$ (= $min\ \{r_v;\ r_a;\ r_{lap};\ r_j;\ r_{pn}\}$ expresses the weakest shear mechanism of an individual column corresponding to the most common premature modes of failure (prior to the flexural one), i.e. shear failure, r_v, anchorage failure, r_a, failure at lap splices, r_{lap}, joint failure, r_j, and punching failure in cases of slabs without beams, r_{pn}. It is determined as the fraction between the base shear force at the occurrence of the controlling mode of failure of the column, $V_{u,lim}$, and the base shear corresponding to the onset of yielding of column reinforcement, $V_{y,flex}$; i.e. $r_{u,lim}=V_{u,lim}/V_{y,flex}$. The expressions for the various strength ratios are presented in Appendix A [2].

In case that beam yielding occurs prior to column failure, $r_{by}<r_{u,lim}$, then the shear force input to the column is limited by yielding of the adjacent beams. In case that interstorey drift demand is $\Theta_i<\Theta_{y,nom,i}^{b}/(1-\lambda_c)$, where $\Theta_{y,nom,i}^{b}$ is the average nominal drift at yielding of beams, then the structure may be assumed to be in the elastic (pre-yielding state). Otherwise, i.e. $\Theta_i>\Theta_{y,nom,i}^{b}/(1-\lambda_c)$, ductile plastic hinging in the beams may develop [2].

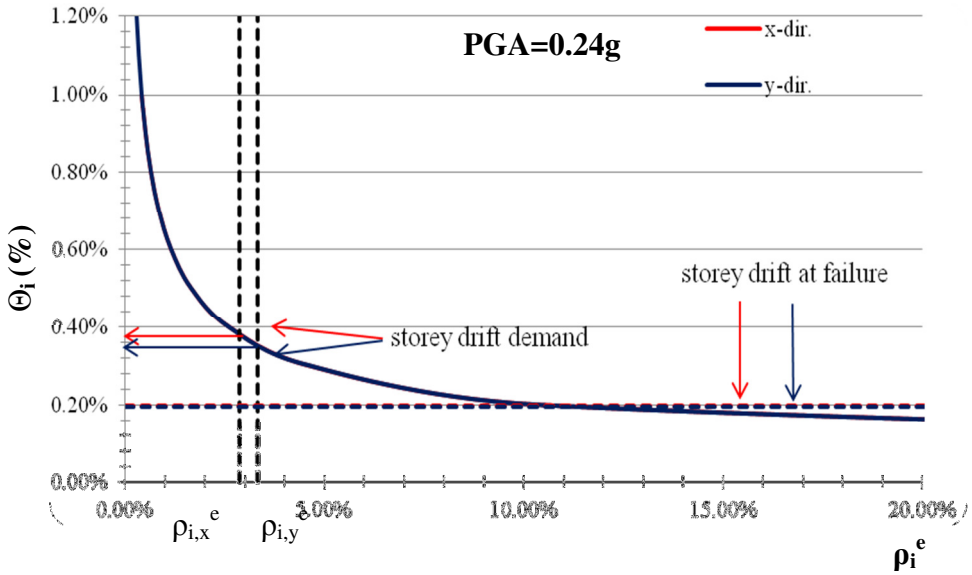

Figure 3: Vulnerability curve.

3.4 Assessment using the Interstorey Drift Spectra (IDS)

The use of the IDS as an efficient design tool for rapid preliminary assessment is illustrated in Fig. 3. First, the period of the building in each direction is estimated according to Eq. (3) and the IDS is plotted according to Eqs. (7) by selecting the adequate range of periods (in Fig. 3 the red curve corresponds to x direction, whereas the blue curve to y direction). The second step involves the estimation of the equivalent vertical members area ratio, ρ_i^e, for each direction of the building. This is depicted in the graph of Fig. 3 by the two vertical black dashed lines (the left dashed black line refers to direction x and the right one to direction y). The intersection of the dashed black line with the vulnerability curve determines the drift demand, Θ_i, per direction. This value is compared to the drift at failure of each direction, shown by the horizontal dashed lines in Fig. 3 (red colored line refers to x direction, whereas the blue colored line to y direction). As it is observed, the storey drift at failure is below the storey drift demand, $\Theta_i<\Theta_{fail,i}$, implying that failure is anticipated in both directions.

4 IMPLEMENTATION OF THE ASSESSMENT METHODOLOGY

4.1 Description of the building

The building studied is an 8-storey residential R.C. building with basement constructed in the center of the city of Thessaloniki (Greece) in 1951 with the first storey (ground floor) used as a commercial space (Fig. 4). The top floor is formed as a setback including two apartments and the end of the stairwell. The typical floor's area is 190.18 m^2, while the first floor's is 172.199 m^2 and the setback's is 160.58 m^2. The building is symmetric along y axis, thus information is provided only for the columns on the left handside. Note that columns C1, C2, C1', C2' (Fig.4) do not continue to the last floor. The building's total height from the ground level is 26.90 m, whereas the individual storey heights are 3.30 m for the 1st, 2nd and 3rd storey, 3.20 m for the 4th, 5th and 6th storey, and 3.00 m for the7th and 8th storey. The basement's height is 2.70 m. However, the columns at the perimeter of the building are captive with clear height 1.4 m (this is the height above the ground level).

It is highlighted that there are two skylights along the building height as well as a stairwell almost in the middle of the floor plan introducing a discontinuity in mass and stiffness distribution and consequently in stress distribution.

The materials considered were B120 concrete quality [3] (f_{ck}=10 MPa was taken in the application of the methodology) and smooth StI [4] for longitudinal and transverse reinforcement of the structural members (f_{yk}=220 MPa was taken). The slab thickness was 0.10 m constant at all floors.

Columns longitudinal reinforcement comprised smooth bars of 14 mm ÷ 20 mm diameter. The longitudinal reinforcement area ratio over the column section ranged between 6.5‰÷9‰ approximately. Column transverse reinforcement comprised rectangular stirrups of 6 mm diameter spaced at 170 mm ÷ 240 mm anchored with 90° hooks in the ends. Concerning longitudinal bars anchorage lengths and lap splices lengths the assumption of 1.00 m and 0.40 m, respectively, was made (consequent with the state of practice from the building's era of construction) lacking any official information. Details regarding column cross section dimensions and amount of longitudinal reinforcement are shown in Table B (Appendix B).

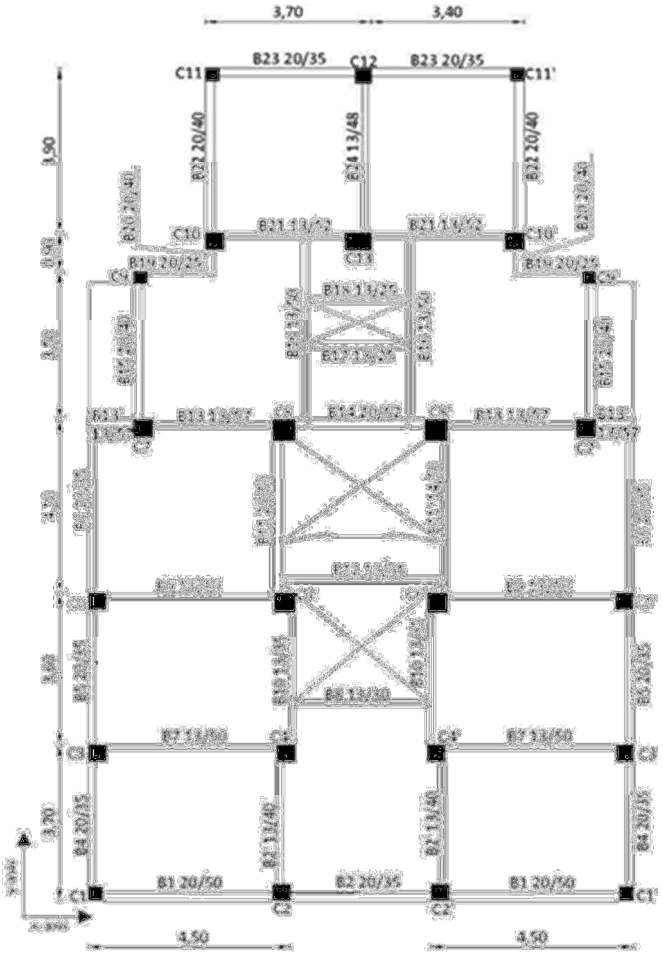

Figure 4: Typical floor plan configuration of the building.

Beams longitudinal reinforcement comprised smooth bars of diameter equal to 10 mm ÷ 18 mm. Note that in a few beams three different bar diameters are placed (e.g. 10 mm, 12 mm and 14 m). The longitudinal reinforcement area ratio ranged between 3.6‰ ÷ 17‰ approximately. Transverse reinforcement comprised rectangular stirrups of 6 mm diameter spaced at 150 mm anchored with 90° hooks in the ends.

Slab dead loads comprise self – weight (24.00 kN/m^3 was assumed as per the initial design of the building) and finishings load (0.60 kN/m^2); slab live load of 2.00 kN/m^2 was assumed. Beams were considered to carry their self - weight and the weight of the masonry infills. An average masonry wall height of 2.80 m was assumed. For external masonry infill walls a 0.20 m thickness was considered leading to 11.20 kN/m vertical dead load distributed onto the external beams. The internal beams are considered to carry the weight of the internal masonry walls of 0.10 m thickness, thus 5.60 kN/m uniform load was distributed on the internal beams. Balcony load was applied as uniform load on the external beams B15 (Fig. 4) giving an additional dead load of 3.40 kN/m and live load of 5.00 kN/m.

4.2 Application of the methodology

The average nominal drift at yield was estimated, $\Theta_{y,nom}^{c}$, and was reduced by the average strength index, $r_{u,lim}$, in order to estimate the average column drift at failure Θ_{fail}^{c} (see section 3.3). This procedure was repeated for each storey in both directions and the results are presented in Table 3 for both directions.

Direction	Parameters	1st	2nd	3rd	4th	5th	6th	7th	8th
x-x	$V_{u,lim}$ (kN)	45.14	30.97	33.76	28.16	20.93	14.30	9.88	8.40
	$V_{y,flex}$ (kN)	92.98	79.51	64.81	50.47	35.06	23.01	16.33	10.79
	$r_{u,lim}$	0.46	0.46	0.49	0.53	0.57	0.59	0.58	0.76
	$\Theta_{y,nom}{}^{c}$	0.24%	0.25%	0.26%	0.28%	0.30%	0.33%	0.32%	0.33%
	$\Theta_{fail}{}^{c}$	0.10%	0.11%	0.13%	0.14%	0.17%	0.20%	0.19%	0.24%
	r_{by}	0.20	0.23	0.29	0.39	0.57	0.86	1.27	1.89
	Failure*	X	X	X	X	X	√	√	√
y-y	V_{min} (kN)	38.34	33.28	28.74	23.45	17.46	12.00	8.46	7.32
	V_{flex} (kN)	89.41	77.33	62.97	47.87	33.21	22.06	16.33	10.79
	$r_{u,lim}$	0.40	0.41	0.43	0.46	0.50	0.52	0.50	0.66
	$\Theta_{y,nom}{}^{c}$	0.24%	0.25%	0.27%	0.28%	0.31%	0.34%	0.32%	0.33%
	$\Theta_{fail}{}^{c}$	0.09%	0.10%	0.11%	0.13%	0.15%	0.17%	0.16%	0.22%
	r_{by}	0.20	0.24	0.29	0.38	0.53	0.79	1.15	2.02
	Failure*	X	X	X	X	√	√	√	√

* *X corresponds to beam yielding ($r_{u,lim} > r_{by}$), √corresponds to column failure*

Table 2: Strength assessment results per storey.

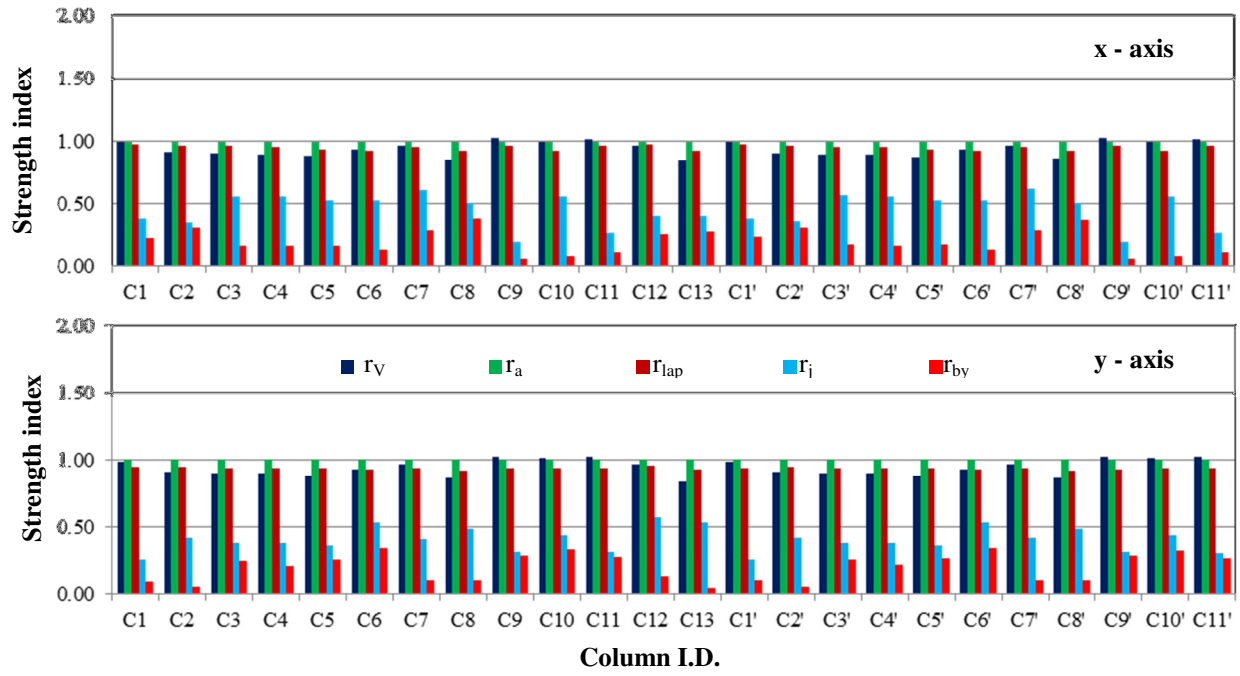

Figure 5: First storey column strength assessment along x – axis and y – axis.

The weakest column resistance mechanism as shown in the graphical representation of the various strength indices in Figs. 5, 6 and 7 for the first, fifth and sixth floor, respectively, is detected in the region of joints. Thus in most cases $r_{u,lim}$ is equal to r_j indicating the insufficient reinforcement detailing and confinement of joints. This mode of failure may be suppressed if the shear force input to the column is limited by yielding of the adjacent beams (i.e. $r_{u,lim} > r_{by}$). This is the case in the first till the fourth storey (Table 2). Column failure is expected in the rest of the storeys as shown by the tick marks in Table 2.

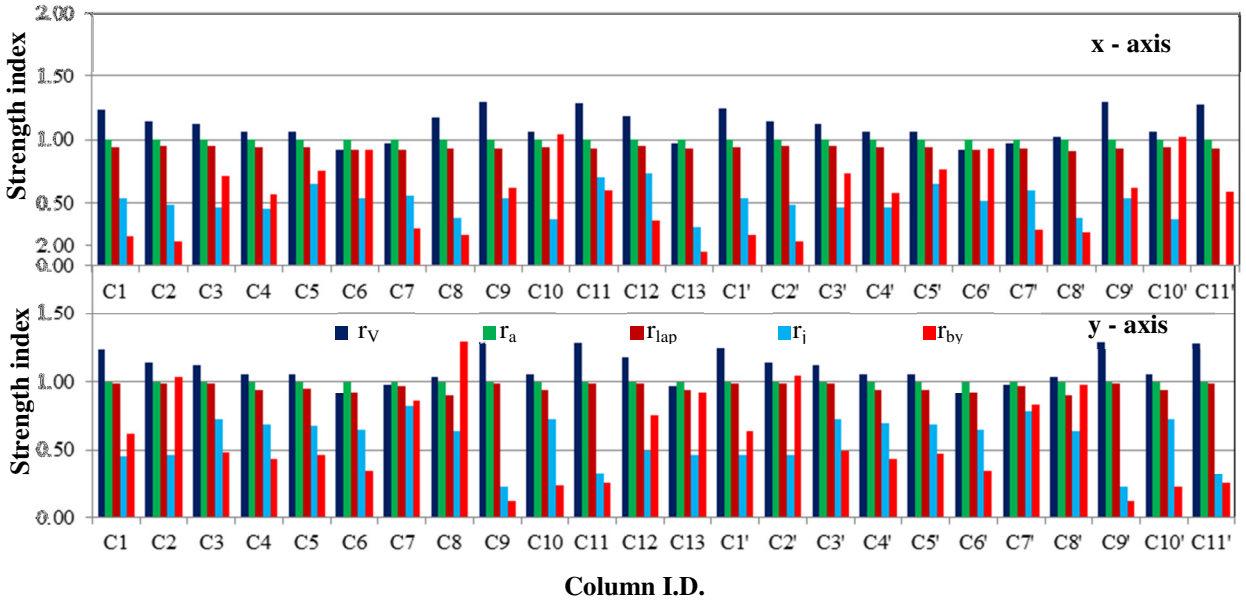

Figure 6: Fifth storey column strength assessment along x – axis and y – axis.

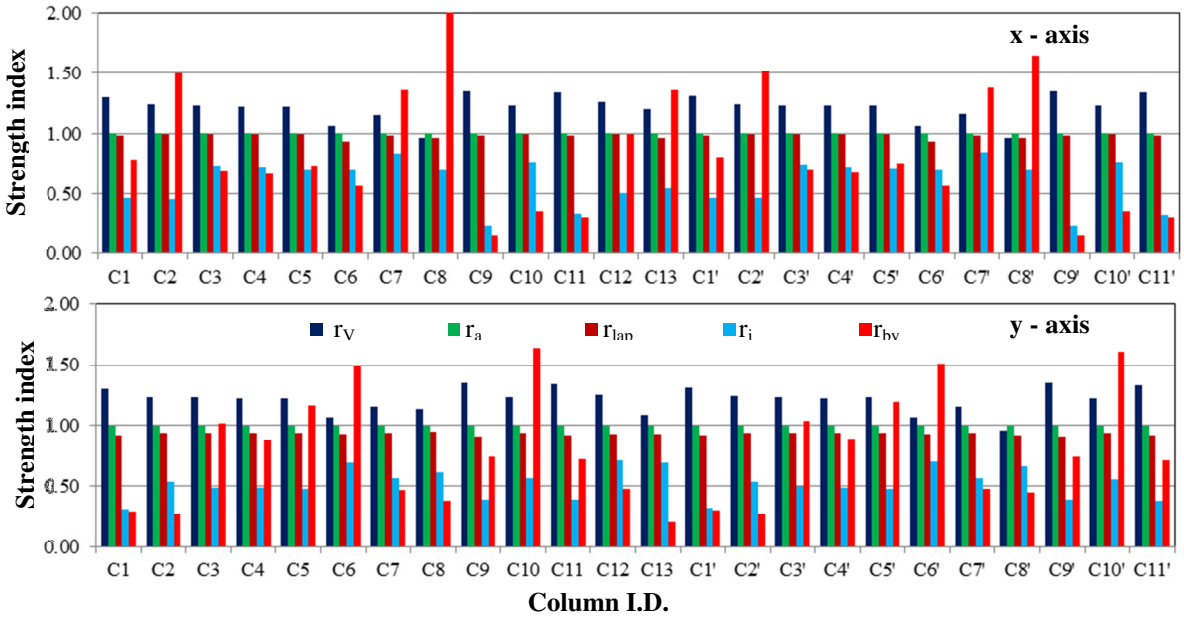

Figure 7: Sixth storey column strength assessment along x – axis and y – axis.

However, only the grey marked values in Table 3 are taken into consideration and used in assessment due to the fact that failure is not expected up to the 4th storey.

Stiffness assessment follows where the buildings's generalized mass and stiffness were estimated and the period in each direction was specified. After implementing the equation $M^* = \sum [N_{(G+0.30Q)} \cdot n/g \cdot \Delta\Phi_i^2]$, where $N_{(G+0.30Q)}$ is the total vertical load of the seismic load combination *(1.00G + 0.30Q)* at the base of all columns of every storey, n is the number of storeys, g = 9.81 m/s^2 is the gravity acceleration and $\Delta\Phi_i^2$ the difference in the response profile between successive storeys, the generalized mass results in M^* = *844.12 t*. The building's generalized stiffness was defined by $K^* = \sum K_i \cdot (\Phi_i - \Phi_{i-1})^2$, where $K_i = V_{min}/(2\theta_{fail}^c \cdot L_s)$

is stiffness at the initiation of failure of each column of the storey, *i*. Thus, $K_x^* = 21380.66$ *kN/m* and $K_y^* = 18220.75$ *kN/m* correspond to $T_x = 1.25$ *s* and $T_y = 1.35$ *s*, respectively. It is reminded that the lateral response shape adopted is that of the shear-type buildings (Eq. (5), Fig. 2).

Considering an average value of coefficient λ_c per storey Θ_{fail} is estimated as shown in Table 3.

Direction	Parameters	1st	2nd	3rd	4th	5th	6th	7th	8th
x-x	λ_c	0.36	0.40	0.45	0.52	0.61	0.69	0.71	0.70
	Θ_{fail}	0.28%	0.27%	0.27%	0.26%	0.27%	0.28%	0.26%	0.34%
y-y	λ_c	0.36	0.40	0.45	0.52	0.61	0.69	0.71	0.70
	Θ_{fail}	0.28%	0.27%	0.27%	0.26%	0.26%	0.26%	0.24%	0.32%

Table 3: Storey drifts at failure.

The column area ratio, $\rho_{c,i}$, and masonry walls area ratio, $\rho_{wm,i}$, are presented in Table 4. As it is observed $\rho_{c,i}$ is identical in both directions in all the storeys, whereas $\rho_{wm,i,y}$ in y direction is almost two and a half times higher than $\rho_{wm,i,x}$ in x direction. The equivalent area ratio of the vertical members in the floor plan ρ_i^e was also estimated (Table 4).

Area ratio (%)	1st	2nd	3rd	4th	5th	6th	7th	8th
$\rho_{c,i}$	2.08	1.87	1.70	1.43	1.15	0.92	0.82	0.85
$\rho_{wm,i,x}$	1.38	1.38	1.38	1.38	1.38	1.38	1.38	1.69
$\rho_{wm,i,y}$	3.63	3.67	3.67	3.67	3.67	3.67	3.67	4.32
$\rho_{i,x}^e$	2.48	2.32	2.20	1.98	1.83	1.77	1.67	1.89
$\rho_{i,y}^e$	3.20	3.11	3.07	2.97	3.05	3.27	3.07	3.50

Table 4: Vertical component's area ratios per direction and storey.

IDS were constructed for two levels of seismicity with PGA = 0.16g and PGA = 0.36g according to Eq. 7(b) (Fig. 8). The vulnerability curves have been plotted for the 1st, 5th and 6th storey. Since the response of the building (beam yielding occurs first) is the same up to the 4th storey, only the IDS of the 1st storey is shown in Fig. 8. In case of the 5th storey the response is differentiated for each direction as depicted in Fig. 8. From the 6th floor and upwards column failure is expected and the vulnerability curve corresponding to the 6th floor is considered representative (Fig. 8).

For the 1st storey and PGA=0.16g (Fig.8(a)) drift demand was estimated along x and y direction equal to Θ_1= 0.25% and 0.22%, respectively. No damage is expected since $\Theta_1 < \Theta_{fail}$ (Table 3). On the contrary, for PGA = 0.36 g (Fig.8(b)) drift demand was estimated along x and y direction equal to Θ_1= 0.56% and 0.51%, respectively. Column failure is anticipated since $\Theta_1 > \Theta_{fail}$. The same procedure was followed for the 5th and 6th storey, the results of which are presented in Tables 5 and 6.

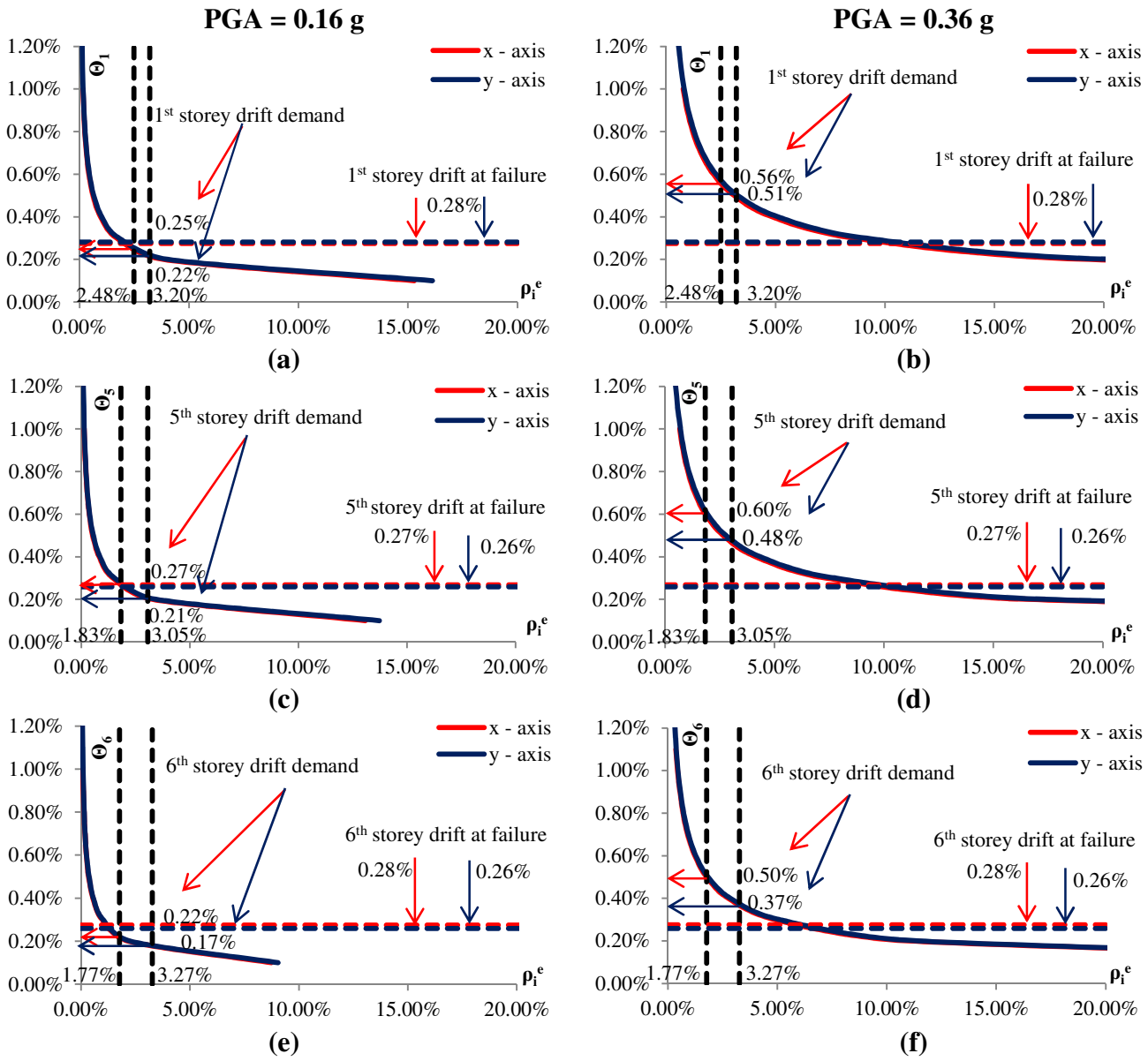

Figure 8: Vulnerability curves (a); (b) of the 1st storey for PGA=0.16g and PGA=0.36g, respectively; (c); (d) of the 5th storey for PGA=0.16g and PGA=0.36g, respectively; (e); (f) of the 6th storey for PGA=0.16g and PGA=0.36g, respectively (red and blue colored lines refer to direction x and y, respectively).

PGA	Dir.	Θ_5	Θ_5^c	Θ_5^b	Beam yielding	θ_{pl}^b	θ_{fail}^c	Column failure
0.16g	x	0.27%	0.17%	0.10%	×	-	0.17%	×
	y	0.21%	0.12%	0.09%	×	-	0.15%	×
0.36g	x	0.60%	0.38%	0.22%	√	0.05%	0.17%	√
	y	0.48%	0.28%	0.20%	×	-	0.15%	√

Table 5: Assessment results for the 5th storey of the building study (√: yes, ×: no).

PGA	Dir.	Θ_6	Θ_6^c	Θ_6^b	Beam yielding	θ_{pl}^b	θ_{fail}^c	Column failure
0.16g	x	0.22%	0.16%	0.06%	×	-	0.20%	×
	y	0.17%	0.11%	0.05%	×	-	0.17%	×
0.36g	x	0.50%	0.36%	0.14%	×	-	0.20%	√
	y	0.37%	0.25%	0.12%	×	-	0.17%	√

Table 6: Assessment results for the 6th storey of the building study (√: yes, ×: no).

5 VALIDITY OF THE RAPID EVALUATION METHODOLOGY THROUGH DETAILED ANALYSES

In order to verify the validity of the rapid evaluation methodology detailed analyses were performed including eigenvalue and pushover analyses. For this purpose a finite element program for static and dynamic analyses of structures SAP2000 Nonlinear Version 15 was used. Two groups of models were created (Fig.9): (i) Model A represents the bear structural system with the presence of external masonry infill walls of thickness t = 0.20 m and height equal to 1.40 m in order to model the captive (or short) column formation at the basement (free storey height is 1.30 m. The free lengths of the columns between successive spans may be characterized as captive columns) and (ii) Model B represents the masonry infilled frame building with external masonry infill walls of thickness t = 0.20 m along its height.

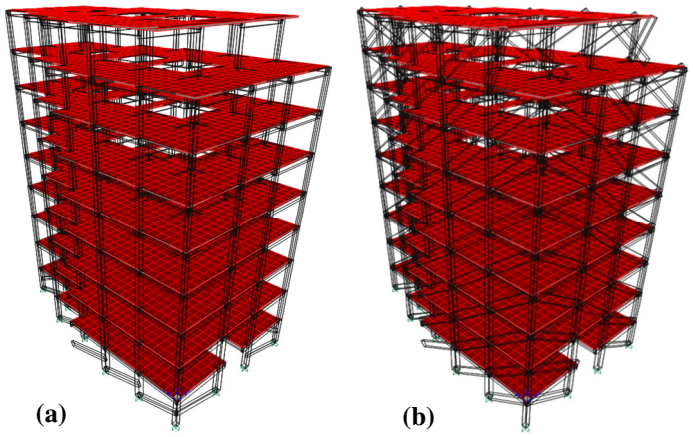

Figure 9: (a) Models A with no masonry infill walls but at the basement of the building; (b) Models B with masonry walls along the height of the building.

5.1 Modeling assumptions

A three-dimensional model of the structure was created in SAP2000 Version 15 where beams and columns were modeled as nonlinear frame elements, whereas shell elements were chosen to model slabs. Masonry infill walls were modeled as diagonal struts using linear frame elements rendering the assignment of their inelastic response more convenient.

Three different materials were defined. Material "Concrete" with mass per unit volume 24.00 kN/m^3, modulus of elasticity E_c=22 GPa [6] and compressive strength f_c =10 MPa [9]; material "Steel" with modulus of elasticity E_s=210 GPa, yield stress f_y=220 MPa and ultimate tensile stress f_u=330 MPa; material "Wall" with zero mass per unit volume (due to the fact that masonry vertical loads were distributed onto the subjacent beams and had already been assigned), modulus of elasticity E_w = 1.25 GPa were characterized.

The cross section dimensions along with the longitudinal and transverse reinforcement were assigned for both columns and beams (information regarding the columns' characteristics appear in Table B, Appendix B). Masonry infill walls were modeled as struts of rectangular cross section with t=0.20 m width by $0.15L_d$ depth [8] where $L_d=\sqrt{L_h^2+h_w^2}$ is the length of the diagonal strut calculated as the square root of the sum of the square of masonry wall horizontal length plus the square of its height. The loads applied were defined in section 4.1.

Elements (beams and columns) inelastic behavior was introduced by the assignment of moment – curvature plastic hinges at their ends. Two different cases were investigated: (i) the "default" plastic hinges whose properties were automatically defined by the program, and (ii) the "user defined" plastic hinges where moment – curvature diagrams were estimated separately for each element. In the case of the "default" plastic hinges interaction of compression N and biaxial flexure M2 and M3 was selected for columns since it represents more precisely their actual state of stress and uniaxial flexure M3 for beams. Note that the option "default" plastic hinges (defined automatically by the program) involves the automatic determination of the moment - curvature (M-phi) diagram for every cross section.

The properties of the "user defined" plastic hinges were estimated by first deriving the moment – curvature diagrams with the use of the sectional analysis program Response 2000 [10] considering interaction between compression N and uniaxial flexure M3 or M2 for columns. In case of beams only uniaxial flexure M3 was considered (Fig. 10). Bilinearization of the moment – curvature diagrams was done with the use of Bilin [11] (Fig. 10).

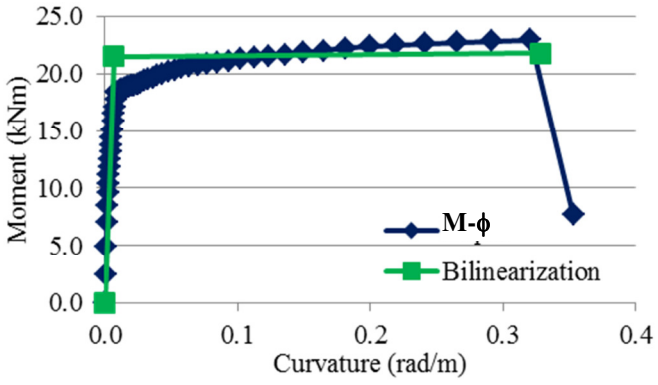

Figure 10: Example of moment – curvature diagram – Bilinearization of M-phi diagram by BILIN.

Plastic hinges were assigned at column and beam ends (Fig.11). The location of the plastic hinges is defined in Fig. 11. The plastic hinge at the column base was assigned at a distance from the joint equal to (h_f/2 + l_p/2), where h_f =0.10 m is the slab thickness and l_p =0.50h the

hinge length [12] (h the column section depth). Considering the top of the column, plastic hinge was assigned at a distance (h_i - h_{beam}^{ave} + $h_f/2$ - $l_p/2$) m from the joint, owing to the fact that column ends were defined in slabs middle plane. Plastic hinges at the left handside of beams were assigned at a distance ($h_c/2$ + $l_p/2$), where h_c is the column section depth and at the right handside at a distance (L_{beam} – $h_c/2$ - $l_p/2$), where L_{beam} the beam length.

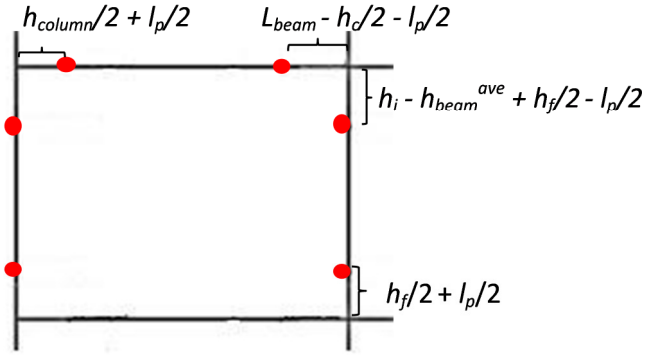

Figure 11: Plastic hinges locations.

Furthermore, the simultaneous existence of plastic and shear hinges was investigated since the model has to be capable of capturing the case of premature column failure, as it was observed in the upper storeys after applying the proposed rapid assessment methodology. Thus, shear hinges were introduced in order to depict this brittle mode of failure usually encountered in structures designed and constructed according to pre – modern code regulations. The value of shear force controlling the shear hinge development is the minimum of the values corresponding to each of the most common premature types of failure (Section 3.3, Appendix A). Shear hinges were assigned only to the column ends of those storeys were column failure prior to beam yielding is expected to occur according to the outcome of the rapid assessment methodology.

Model		Default hinges	User defined hinges	Shear hinges
A (bear frame building)	A.1.1.	√		
	A.1.2.	√		√
	A.2.1.		√	
	A.2.2.		√	√
B (masonry infilled frame building)	B.1.1.	√		
	B.1.2.	√		√
	B.2.1.		√	
	B.2.2.		√	√

Table 7: Definition of the various models examined.

Depending on the type of plastic hinges (automatic or user defined) and the existence or not of shear hinges, eight different analytical models result (Table 7). The identification code of each model follows the notation K.L.M. where K stands for Model A (with external masonry walls only in the lower half height of the basement) or Model B (external masonry infills throughout the building), L receives values “1” for default plastic hinges or “2” for user defined plastic hinges and M receives values “1” stands for M – ϕ plastic hinges whereas

value "2" stands for both M – ϕ and shear hinges. Thus, the models studied are A.1.1, A.1.2, A.2.1, A.2.2, B.1.1, B.1.2, B.2.1 and B.2.2 (Table 7). For instance, model A.2.1 comprises basement external masonry walls and user defined plastic hinges M – ϕ. It should be reminded that eigenvalue and pushover analyses have been performed for all the above cases.

5.2 Eigenvalue analysis

Cracked sections were considered for columns and beams with a 50% reduction of their moment of inertia. In Figs. 12 and 13, the results of the eigenvalue analyses for the first three modes are presented. Information relative to the deformed shapes, the eigenperiods and the mass participation ratios appear.

Models A: The first mode shape for Models A is purely rotational; the second one purely translational towards the stronger axis of the structure (y – axis) while the third one is mixed (rotational/translational towards the weaker axis (x - axis)) (Fig. 12). The eigenperiod given in Fig. 12(c) refers to the x – translational component of the third mode.

Models B: For Models B the first mode shape is purely translational towards x - axis; the second one is purely translational towards y – axis ad the third one is purely rotational (Fig.13).

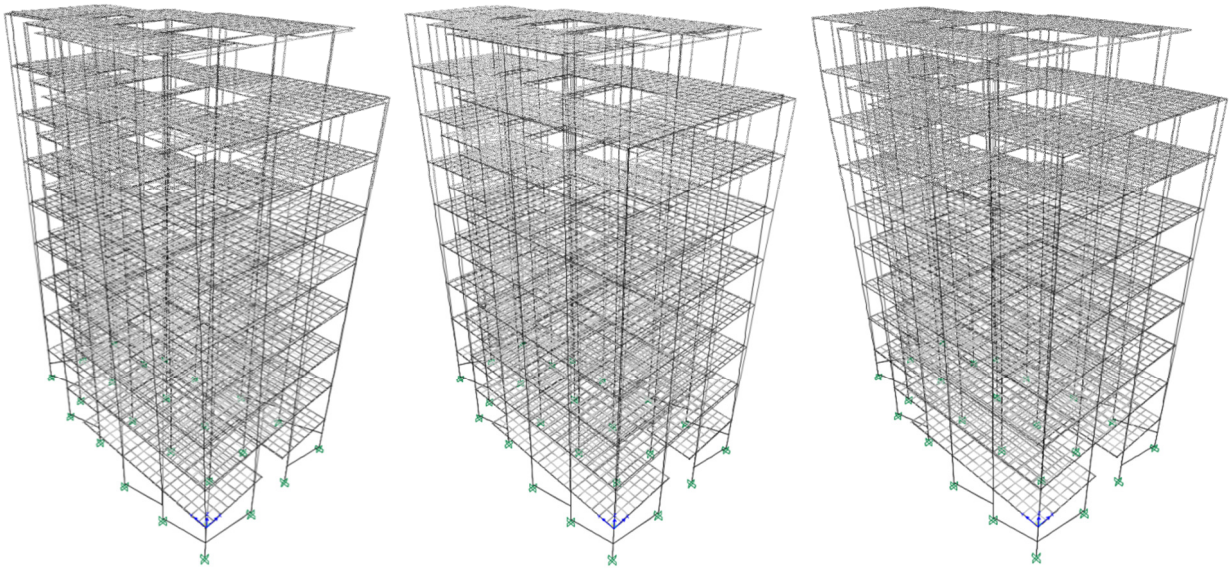

(a) T_1=1.99 s MPMR=1.0% **(b)** T_2=1.98 s MPMR=69.6% **(c)** T_3=1.85 s MPMR=57.6%

Figure 12: Deformed shape; eigenperiod and modal participating mass ratio (MPMR) from 3D eigenvalue analysis for Models A: (a) 1st mode; (b) 2nd mode; (c) 3rd mode.

Translational eigenperiod values of Models B are observed to be decreased in comparison to those of Models A as expected since masonry infill walls increase the structural system's stiffness. Furthermore, comparing eigenperiod values for Models B with those derived by the proposed assessment methodology (It is noted that the frame building responds with its fundamental modal shape) a good correlation is observed. It is reminded that eigenperiod values by the methodology application are T_x =1.25 s and T_y =1.35 s along the weaker and stronger axis of the structure, respectively. The difference recorded is +13% and -24% along x and y axis, respectively, which is considered acceptable given that the first translational mode

in Models B (Figs. 13(a)) is close to the fundamental shape considered in the assessment methodology.

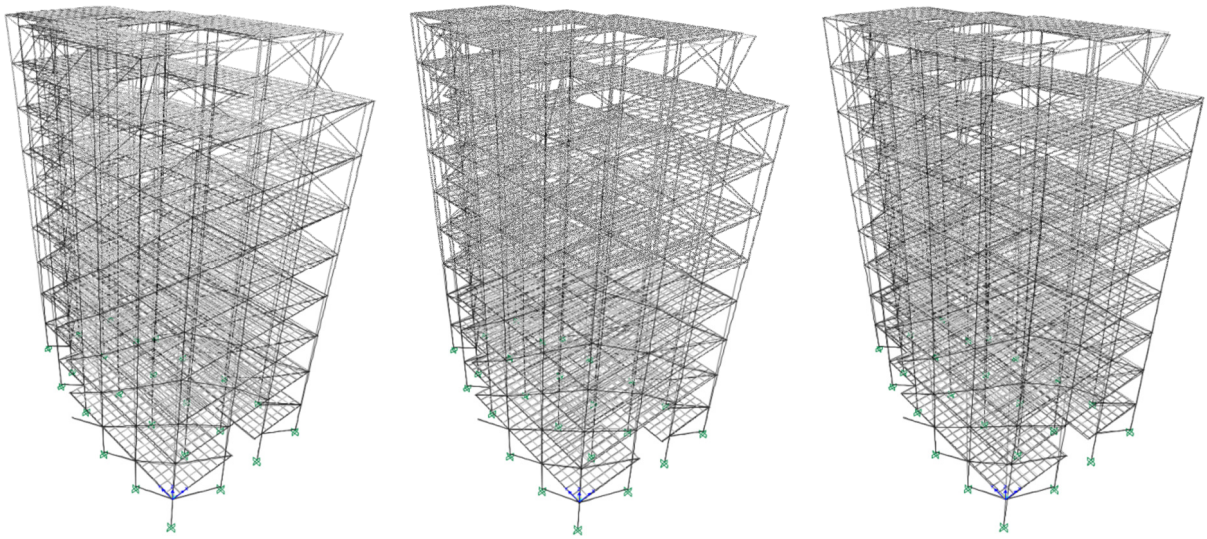

(a) T_1=1.41 s MPMR=74.9%

(b) T_2=1.03 s MPMR=74.3%

(c) T_3=0.92 s MPMR=15.0%

Figure 13: Deformed shape; self - period and modal participating mass ratios (MPMR) from 3D eigenvalue analysis for Models B: (a) 1st mode; (b) 2nd mode; (c) 3rd mode.

5.3 Pushover analysis

The groups of Models A and B were subjected to pushover analyses separately for the two orthogonal directions x and y. Vertical gravity loads and lateral seismic loads were applied simultaneously on the structure. Three different lateral force distribution profiles along the height of the building for each model were investigated (Figs. 14, 15), the modal, the triangular and the uniform shape. In Figs. 14(a), (b) the modal lateral load profile is plotted for Models A along x and y axis, respectively. Similarly, the modal lateral load profile per direction is presented in Figs. 15(a), (b) for Models B. From the pushover analyses conducted, it was shown that response of the structure described by the base shear – roof displacement curve is slightly differentiated for the triangular and modal load pattern. However, uniform distribution led always to more favorable results. For this purpose, it was decided to be presented only the results from the application of the uniform and modal lateral load profile.

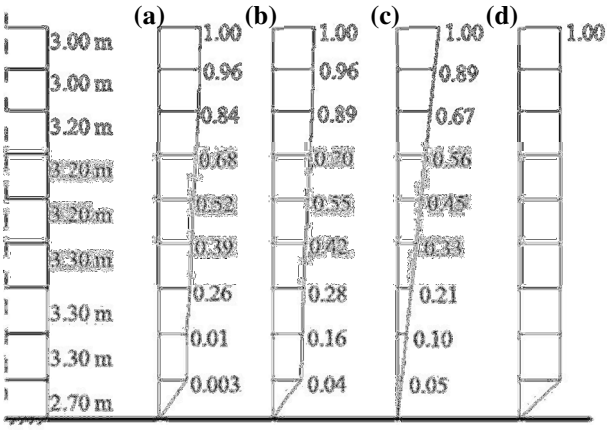

Figure 14: Lateral load profiles for Models a: (a) modal along x - axis; (b) modal along y - axis; (c) triangular (same for both directions); (d) uniform (same for both directions).

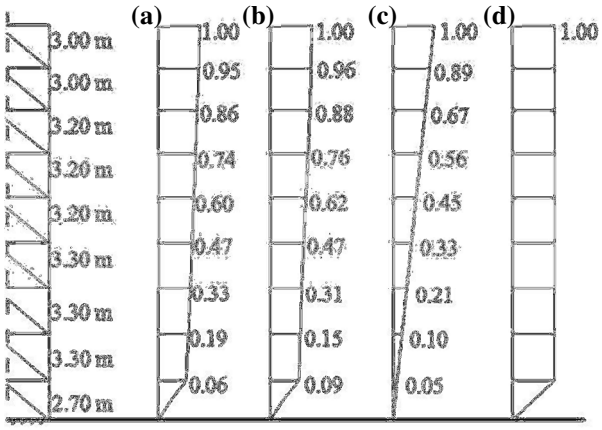

Figure 15: Lateral load profiles for Models B: (a) modal along x - axis; (b) modal along y - axis; (c) triangular (same for both directions); (d) uniform (same for both directions).

5.3.1. Comparison between the different modeling approaches

Model A.2.1. (masonry walls in the basement, user defined M-ϕ plastic hinges): In Fig.16 the pushover curves were plotted for x and y direction for the different load profiles (red colored lines refer to x – axis while blue colored lines refer to y - axis). The difference in the maximum base shear force as well as in the roof displacement between the two lateral load patterns is significant. The maximum base shear force value for uniform load distribution compared to that for the modal lateral force profile is 78% and 20% higher in x and y direction, respectively. As far as the maximum roof displacement attained again the values reached in the case of the uniform load distribution are higher compared to the modal shape load distribution (20% higher along x – axis (Fig.16(a)), and 24% higher in y-axis (Fig. 16(b))). The maximum drift reached at which failure occurs was 0.55% in both x and y directions for uniform load distribution whereas it was 0.45% in both directions for modal load distribution (allaxa th seira). The maximum peak ground acceleration that this model could sustain for the *G+0.3Q* load combination (average normalized axial load ratio v_{ave}=0.45, *W*=16791kN) was 10.3 % (=1729/16791 in the x direction and =1726/16791 in the y direction) of g for the uniform load pattern, whereas it was 5.8% (=973/16791) and 5.4% (=915/16791) of g, in the x and y directions, respectively, for the modal load pattern.

Model A.2.2 (masonry walls in the basement, user defined M-ϕ plastic hinges and shear hinges): The pushover curves derived for the orthogonal directions and the aforementioned load profiles are presented in Fig.17. Like the previous model (A.2.1.), the uniform load distribution results in higher values of maximum base shear force and roof displacement compared to the modal load pattern. Comparing the behavior of Model A.2.1 (without shear hinges, (Fig.16)) to that of Model A.2.2 (with shear hinges, (Fig.17)) it is evident that in the second case the structure failed at much lower levels of base shear. The maximum drift where brittle failure occurred is 0.17% and 0.16% in both x and y directions for the uniform and modal load distribution, respectively. In case that shear hinges were assigned, due to the premature failure of columns well before reaching their state of yielding, the whole building failed after the analysis had completed the first few loading steps. Since shear failure is a brittle mode of failure, the building's capacity to develop inelastic deformation after loss of its load bearing capacity is low. Thus, in pushover curves of this type of models no metelastic branch appears. The maximum peak ground acceleration that this model could sustain for the *G+0.3Q* load combination was 5.9 % (=992/16791) and 5.3% (=888/16791) of g along x and

y directions, respectively, for the uniform load pattern while it was only 3.5% (=583/16791) and 2.8% (=915/16791) of g in the x and y directions, respectively, for the modal load pattern.

From the above, it seems that the strength value assigned to the shear hinges, which corresponds to the weakest column resistance mechanism detected in the region of joints, leads to conservative results. The value of $\underline{r_j}$ is below 0.5 for the majority of the columns, implying that failure occurs when the shear strength reaches 50% of its flexural strength at yield.

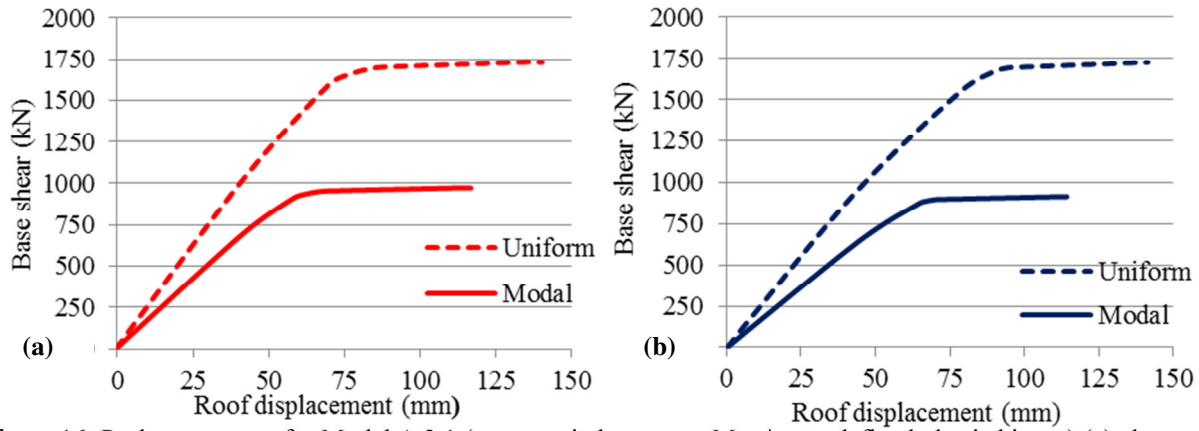

Figure 16: Pushover curves for Model A.2.1 (masonry in basement, M – ϕ user defined plastic hinges) (a) along x axis and (b) y axis.

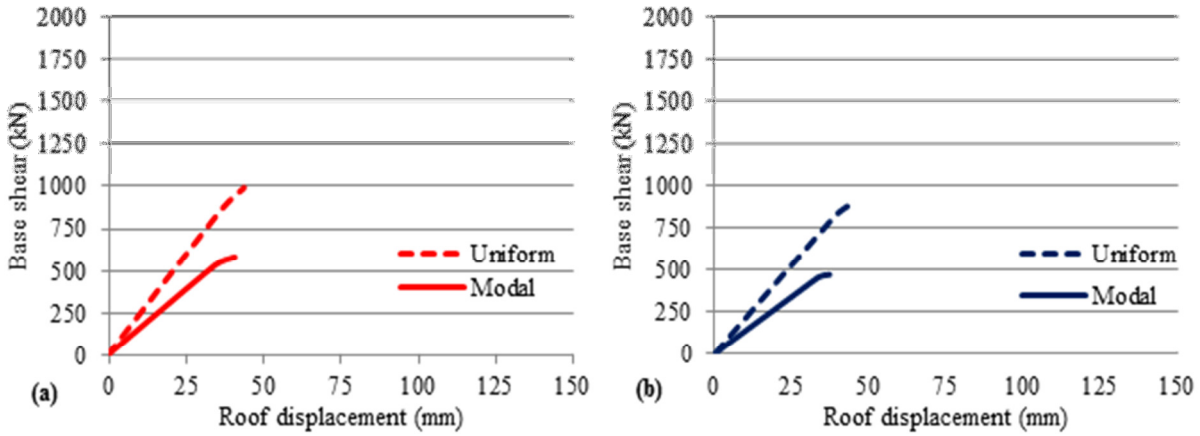

Figure 17: Pushover curves for Model A.2.2 (masonry in basement, M – ϕ user defined plastic hinges and user defined shear hinges) (a) along x axis and (b) y axis.

Model B.2.1. (external masonry infill walls throughout the building, user defined M-ϕ plastic hinges): As it is observed in Fig.18 roof displacement reached higher values along y direction compared to those in x direction due to the larger structural stiffness along y axis drift (the area ratio of masonry infill walls is higher along y – axis, Fig. 9(b)). The maximum drift in which failure occurred was 0.36% and 0.29% in x and y direction, respectively, for uniform load distribution. In case of modal distribution, the maximum drift at failure was 0.38 % and 0.36% in x and y directions, respectively. The maximum peak ground acceleration that this model could sustain for the *G+0.3Q* load combination was 16.8% (=2848/16791) and 20.2% (=3443/16971) of g, along x and y axis, respectively, for the uniform load pattern

whereas it was 13% (=2199/16791) and 18.1% (=3067/16791) of g, along x and y axis, re-respectively, for the modal lateral force profile. The addition of infill walls increased substan-substantially both stiffness and strength of the structural system rendering it capable of tolerating higher levels of peak ground acceleration. Failure of the masonry infill walls limited the deformation capacity of the structure.

Model B.2.2 (external masonry infill walls throughout the building, user defined M-ϕ plastic hinges and shear hinges): The maximum drifts at failure reached for Model B.2.2. were 0.37% and 0.28% along x and y direction for the uniform load pattern and 0.32 % and 0.36% in x and y direction for the modal load profile (Fig. 19). The maximum peak ground acceleration for the *G+0.3Q* load combination was 16.7% (=2833/16791) and 20.3% (=3453/16791) of g along x and y direction for the uniform load pattern. As far as the modal load shape is concerned, the maximum peak ground acceleration was 10.7% (=1814/16791) and 18.1% (=3071/16791) of g in the x and y direction, respectively. Comparing the response of B.2.1 (no shear hinges) and B.2.2. (with shear hinges), it seems that when masonry infills are modeled the assignment of shear hinges has almost no effect on the structural response.

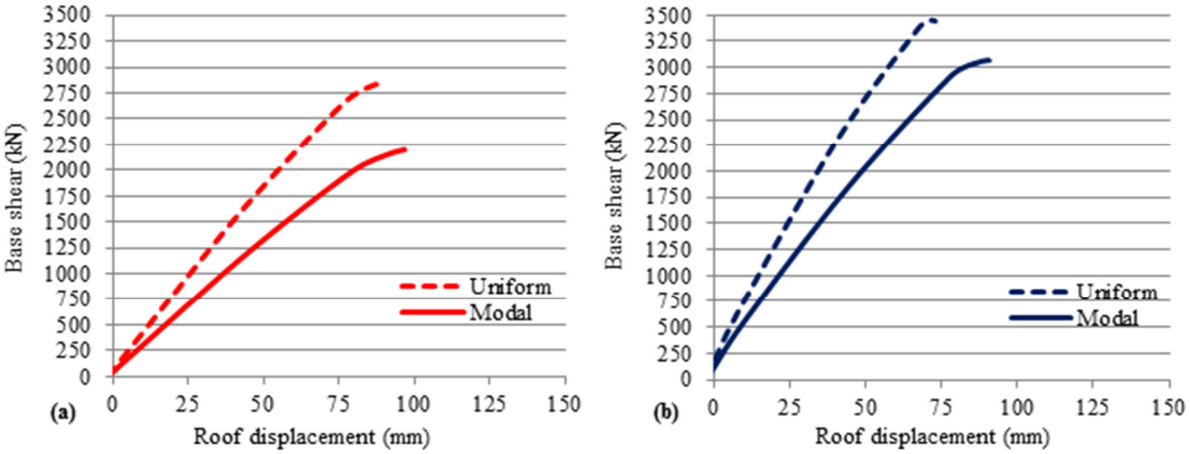

Figure 18: Pushover curves for Model B.2.1 (masonry along the building height, M – ϕ user defined plastic hinges) (a) along x axis and (b) y axis.

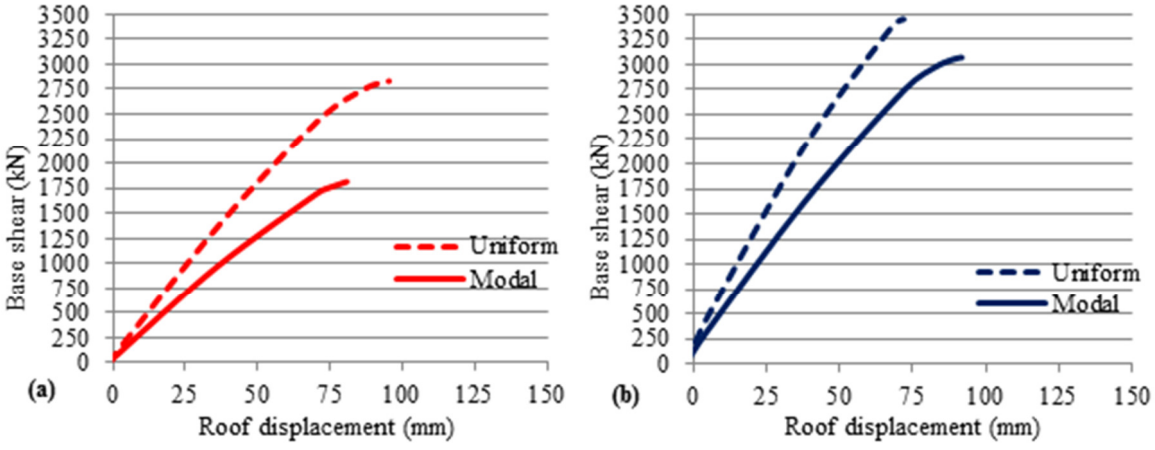

Figure 19: Pushover curves for Model B.2.2 (masonry along the building height, M – ϕ user defined plastic hinges and user defined shear hinges) (a) along x axis and (b) y axis.

5.3.2. Distribution of plastic hinge formation

As it has already been shown, in those models where shear hinges were considered (A.2.2, B.2.2.: user defined hinges and shear hinges), analysis was terminated at low levels of base shear. In order to shed light on the building state before and after failure, the distribution of plastic hinge formation is studied at two levels of drift corresponding to the end point of the elastic branch of the pushover curve (called hereafter "yielding drift") and to the ultimate value of roof displacement (called hereafter "ultimate"). In case of A.2.2., the sequence of plastic hinge formation is presented for drift levels 0.13% and 0.15% in x direction (Fig. 21) and for drift levels 0.12% and 0.14% in y direction (Fig. 22). The masonry infilled building, model B.2.2. is also considered and the drift levels for which the plastic hinge formation is presented are 0.26% and 0.30% in x direction (Fig. 23) and 0.27% and 0.31% in y direction (Fig. 24). The distribution of plastic hinge formation is shown for all the frames in both directions. The frame labeling is presented in Fig. 20.

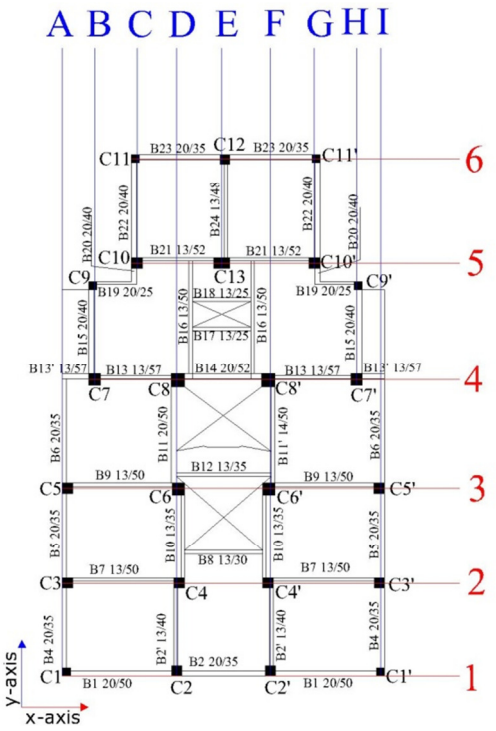

Figure 20: Frames definition.

Model A.2.2. (masonry walls in the basement, user defined M-ϕ plastic hinges and shear hinges):

- Drift at "yielding" (0.13%) x direction: It is observed that at this level of drift, columns in the upper storeys (where shear hinges were assigned) lost their load bearing capacity and failled (red colored plastic hinges) (Fig. 21(a)-(f)). Plastic hinges developed in a few beam ends of the intermediate storeys in Frame 1 and 4 (Fig. 21(a); (d)).
- Drift at "yielding" (0.12%) y direction: Likewise x direction, premature shear failure occurred in most columns of the upper storeys. However, there are a few columns that reached deformations in the post-yield region (blue and turquoise colored plastic hinges) (Fig. 22(a)-(c)). Plastic hinges developed in a few beam ends in the external Frame A (Fig. 22(a)).
- Drift at "ultimate" (0.15%) x direction: Plastic hinges development propagated in a few beam ends of the intermediate and low storeys (Fig. 21(g); (j); (k)) without any alteration in the state of columns. It is observed that except for the upper storeys' columns, neither other columns nor beams yielded or failed.
- Drift at "ultimate" (0.14%) y direction: At this level of drift, shear failure progressed to columns of the upper storeys in Frames B; D and E (Fig. 22(g); (i) and (j)). Furthermore, beams of the intermediate storeys reached their yield state in Frame D (Fig. 22(i)).

Model B.2.2. (external masonry infill walls throughout the building, user defined M-ϕ plastic hinges and shear hinges):

- Drift at "yielding" (0.26%) x direction: It is observed that columns of the upper storeys failled owing to shear failure (the phenomenon was captured by the assignment of shear hinges). In addition, it is significant that two internal columns in Frame 4 (Fig.

23(d)) and one in Frame 5 (Fig. 23(e)) in an intermediate storey yielded. Plastic hinges developed in almost all beam ends of the first four storeys (Fig. 23(a)-(f)). No masonry walls' cracking was observed at this level of drift.

- Drift at "yielding" (0.27%) y direction: Also in this direction and at this level of drift column failure was dominant in the upper storeys. Significant deformation developed in almost all beam ends of the first four storeys (Frames A-E; Fig. 24(a)-(e)). At yielding drift the external masonry panels of the first two storeys cracked (Fig. 24(a)-(c)).
- Drift at "ultimate" (0.30%) x direction: Plastic hinges developped in all the internal columns of the first four storeys (Frames 4 and 5; Fig. 23(j); (k)). Beams' yielding occurred in the lower storeys in all frames. Masonry infill walls of an intermediate storey cracked. The presence of external infill walls prevented damage in the external columns. It is evident that masonry walls contributed to the stiffness of the structural system and in this case they behaved favorably concerning load bearing elements hierarchy of failure.
- Drift at "ultimate" (0.34%) y direction: At ultimate drift the internal columns in the intermediate storeys yielded (Fig. 24(h)-(j)). Concerning external columns their deformation was localized in the first storey. Plastic hinge development in beam ends was not differentiated compared to the "yielding" level of drift. Almost all masonry infill walls cracked. The building along direction y was subjected to higher values of base shear force compared to direction x. Therefore, external column deformation was not prevented in this direction since masonry panels cracked.

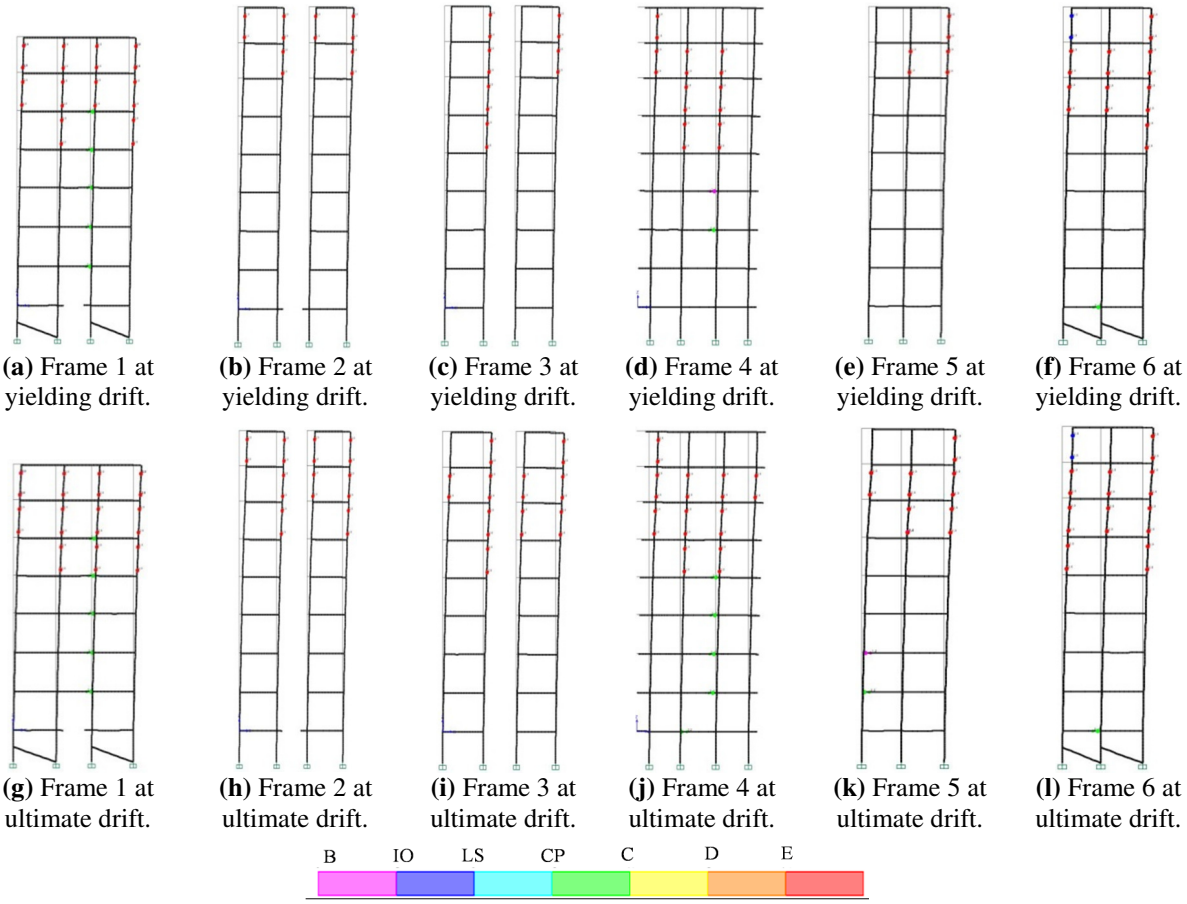

(a) Frame 1 at yielding drift. **(b)** Frame 2 at yielding drift. **(c)** Frame 3 at yielding drift. **(d)** Frame 4 at yielding drift. **(e)** Frame 5 at yielding drift. **(f)** Frame 6 at yielding drift.

(g) Frame 1 at ultimate drift. **(h)** Frame 2 at ultimate drift. **(i)** Frame 3 at ultimate drift. **(j)** Frame 4 at ultimate drift. **(k)** Frame 5 at ultimate drift. **(l)** Frame 6 at ultimate drift.

Figure 21: Distribution of plastic hinge formation in x – direction of Model A.2.2 at yielding and ultimate drift.

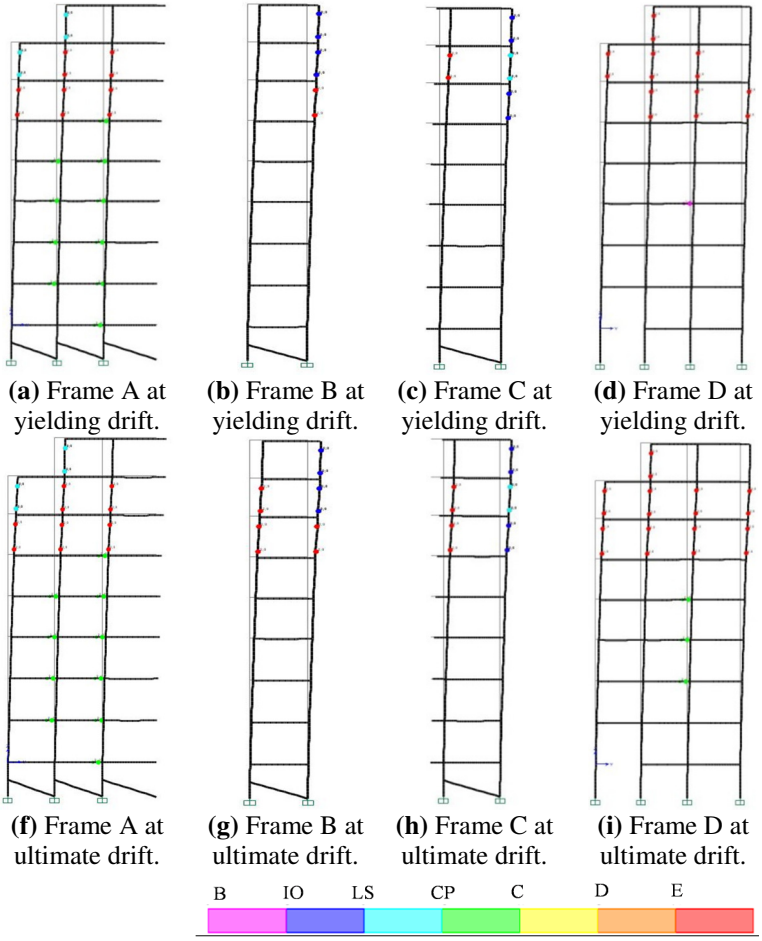

(a) Frame A at yielding drift. **(b)** Frame B at yielding drift. **(c)** Frame C at yielding drift. **(d)** Frame D at yielding drift. **(e)** Frame E at yielding drift.

(f) Frame A at ultimate drift. **(g)** Frame B at ultimate drift. **(h)** Frame C at ultimate drift. **(i)** Frame D at ultimate drift. **(j)** Frame E at ultimate drift.

Figure 22: Distribution of plastic hinge formation in y – direction of Model A.2.2 at yielding and ultimate drift.

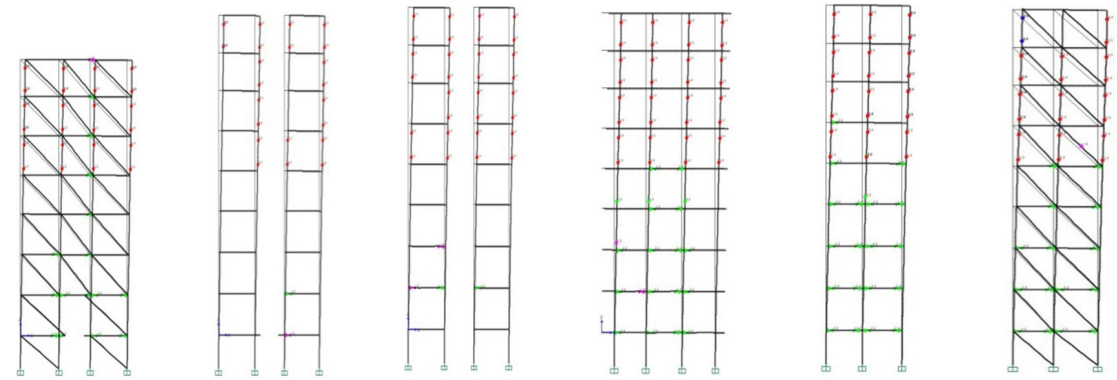

(a) Frame 1 at yielding drift. **(b)** Frame 2 at yielding drift. **(c)** Frame 3 at yielding drift. **(d)** Frame 4 at yielding drift. **(e)** Frame 5 at yielding drift. **(f)** Frame 6 at yielding drift.

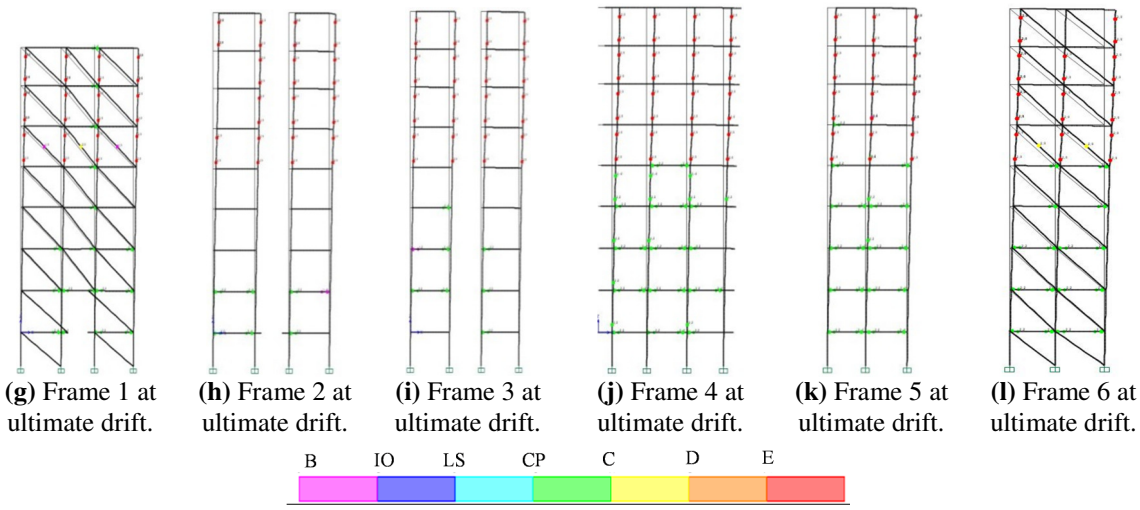

(g) Frame 1 at ultimate drift. **(h)** Frame 2 at ultimate drift. **(i)** Frame 3 at ultimate drift. **(j)** Frame 4 at ultimate drift. **(k)** Frame 5 at ultimate drift. **(l)** Frame 6 at ultimate drift.

Figure 23: Distribution of plastic hinge formation in x – direction of Model B.2.2 at yielding and ultimate drift.

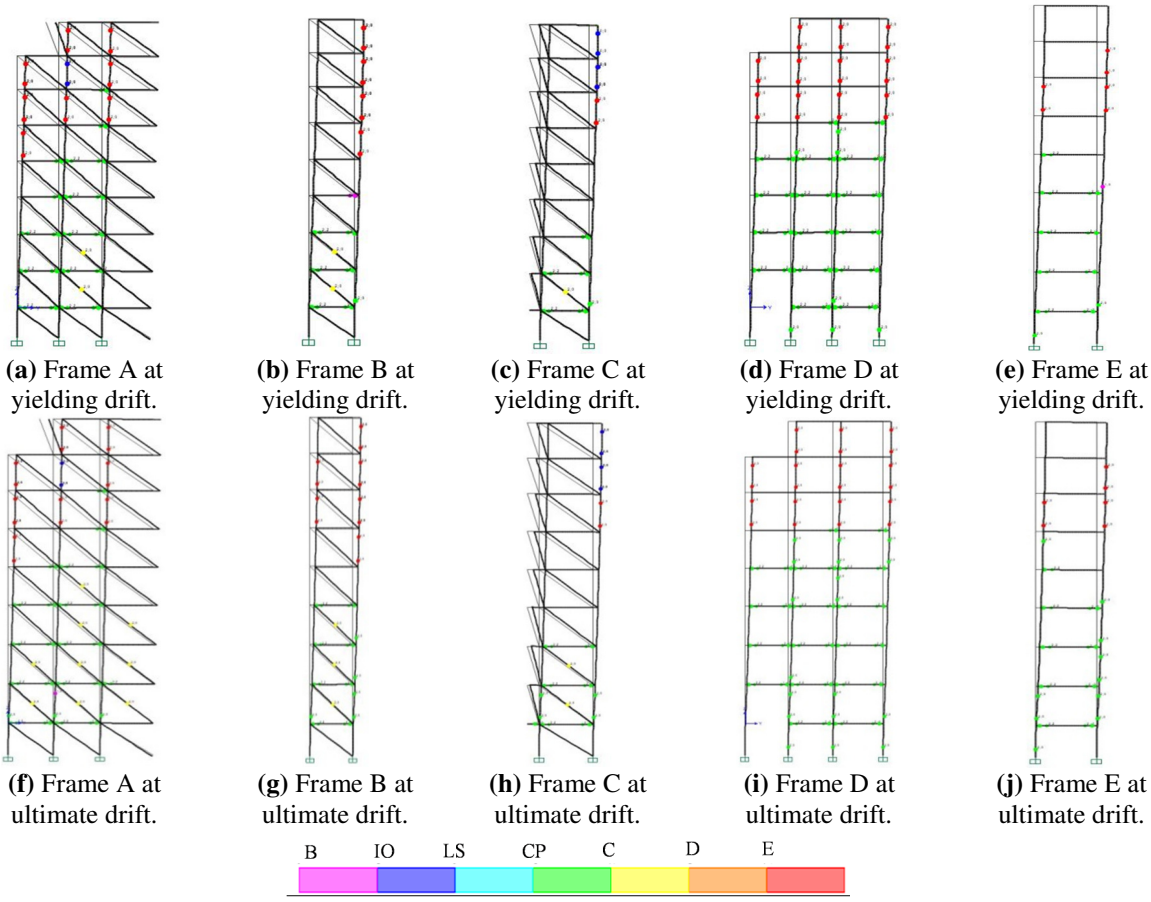

(a) Frame A at yielding drift. **(b)** Frame B at yielding drift. **(c)** Frame C at yielding drift. **(d)** Frame D at yielding drift. **(e)** Frame E at yielding drift.

(f) Frame A at ultimate drift. **(g)** Frame B at ultimate drift. **(h)** Frame C at ultimate drift. **(i)** Frame D at ultimate drift. **(j)** Frame E at ultimate drift.

Figure 24: Distribution of plastic hinge formation in y – direction of Model B.2.2 at yielding and ultimate drift.

6 CONCLUSIONS

A rapid evaluation methodology which renders preliminary assessment of the large inventory of non – ductile multistory RC buildings feasible was presented and implemented in the study conducted herein. Buildings following the pre-modern codes usually designed for gravity loads only without any reinforcement detailing are susceptible to future earthquake events. The proposed methodology requires information of the building's characteristics that are easily accessible, such as the building's geometry in plan and elevation, the number of storeys and their height as well as material properties and geometry and reinforcement of column and beam sections. In case that information relative to cross section detailing is not available, data could be extracted by the construction practice of the era of the building. The methodology establishes two criteria. The strength criterion highlights columns' weakest resistance mechanism under lateral load based on the most common premature modes of failure encountered in vertical load bearing elements with insufficient reinforcement detailing, i.e. shear, anchorage/lap splice, joint failure, the possibility of beam yielding prior to premature column failure is also taken into consideration. Stiffness criterion through the use of the Interstorey Drift Spectra (IDS) and given the estimated equivalent vertical members area ratio estimates the drift demand introduced by the excitation scenario. Assessment is conducted by comparing drift capacity to drift demand. The proposed methodology is recommended to be applied along the height of the building since the 1950's mutlistorey buildings are characterized by in height irregularities in mass and stiffness distribution. Observations made in the database of buildings of that era indicate significant reduction of the dimensions and reinforcement of columns at the upper storeys.

The proposed methodology was implemented in a multistory building constructed in the 1950's in the city of Thessaloniki, Greece. The building was subjected to two seismic scenarios for PGA=0.16g and 0.36g. The results obtained for PGA=0.16g demonstrate building's survival with no damage neither on beams nor on columns. For the second scenario (0.36g), beam yielding and damage localization is anticipated in the first 4 storeys, whereas premature column failure is expected from the 5^{th} to the last storey.

Validity of the proposed methodology was examined by conducting pushover analyses for two groups of models of the building under consideration. The two groups of analytical models are differentiated as per the existence or not of masonry infill walls. Modeling and analyses were performed using SAP2000 v15. Plastic hinges of two types were assigned to beams and columns. The "default" hinges were automatically defined by the program, whereas the user defined hinges properties were determined after sectional analysis. Furthermore, in some of the models shear hinges were also considered additional to the moment –curvature hinges in order to model the premature mode failure of columns.

The results of the rapid assessment methodology are in accordance with the results regarding the analytical model where masonry infill walls, user defined plastic hinges M- phi and shear hinges were considered. The methodology indicated column deficiencies and premature failure in the 3 upper storeys which was verified by the distribution of plastic hinge formation where damage localized in the columns of the 3 last storeys.

In conclusion, the proposed rapid assessment methodology provides a clear insight of the expected mode of failure of existing substandard buildings. The objective of the development of this preliminary assessment methodology is not to substitute detailed analyses but to be used as an efficient tool in order to single out the most deficient and seismic vulnerable that need to be examined further.

REFERENCES

[1] G.E. Thermou, S.J. Pantazopoulou, Assessment indices for the seismic vulnerability of existing RC buildings, Journal of Earthquake Engineering and Structural Dynamics, 40(3), 293-313, 2011.

[2] S.J. Pardalopoulos, G.E. Thermou, S.J. Pantazopoulou, Screening Criteria to Identify Brittle R.C. Structural Failures in Earthquakes, Bulletin of Earthquake Engineering, 11, 607-636, 2013.

[3] RD, Design regulation of reinforced concrete building works. *Royal Decree* (18.2/26.07.1954), Ministry of Public Works, Greece (in Greek), 1954.

[4] Deutsches Institut für Normung (DIN). Beton und Stahlbetonbau: Bemessung und Ausführung. DIN 1045, Berlin, 1936.

[5] Thermou GE, Pantazopoulou SJ, Elnashai AS. Design and assessment models and spectra for repaired reinforced concrete structures. *MAE Center Report*, CD release, 2009; 09–(01).

[6] Eurocode 2. Design of concrete structures—Part 1-1: General rules and rules for buildings. *EN1992-1-2005:E*, European Committee for Standardization (CEN), Brussels, 2004.

[7] Eurocode 8. Design of structures for earthquake resistance—Part 1: General rules, seismic actions and rules for buildings. *EN1998-1-2004:E*, European Committee for Standardization(CEN), Brussels, 2004.

[8] KANEPE, Interventions Code (of Greece). Earthquake Planning and Protection Organization (E.P.P.O.), 2012 (in Greek).

[9] Federation of Structural Concrete (fib). Seismic assessment and retrofit of reinforced concrete buildings. fib Bulletin 24 State-of-art report prepared by Task Group 7.1, 2003.

[10] Evan Bentz and Michael P. Collins, Response 2000, User manual, V. 1.1. September 2001.

[11] G. Panagopoulos, A.I. Kappos, Bilinear approximations of force-displacement curves, 16^{o} Concrete Conference, 21-23/10/2009, Pafos, Cyprus.

[12] Park R, Paulay T., Reinforced concrete structures. New York: John Wiley & Sons; 1975. 769 pages.

[13] ACI-ASCE Committee 352. Recommendations for Design of Beam-Column Connections in Monolithic Reinforced Concrete Structures, American Concrete Institute, Farmington Hills, MI, 2008.

APPENDIX A

The expressions for strength indices are presented below [2].

Shear strength ratio is defined as:

$$r_v = \frac{\nu \cdot \tan a \cdot b \cdot d \cdot f_c^{'} + A_{st} \cdot f_{st} \cdot \frac{d - \xi \cdot d}{s} \cdot \cot \theta_1}{\left[\rho_{\ell,tot} \cdot \frac{f_s}{f_c^{'}} \cdot (1 - 0.40 \cdot \xi) + \nu \cdot \left(\frac{h}{d} - 0.80 \cdot \xi \right) \right] \cdot \frac{b \cdot d^2 \cdot f_c^{'}}{h_{st}}} \Leftrightarrow$$

$$r_v = \frac{\nu \cdot \left(\frac{h}{d} - 0.80 \cdot \xi \right) + \frac{A_{st}}{b \cdot d} \cdot \frac{f_{st}}{f_c^{'}} \cdot \frac{h_{st}}{d} \cdot (1 - \xi) \cdot \cot \theta_1 \cdot \frac{d}{s}}{\rho_{\ell,tot} \cdot \frac{f_s}{f_c^{'}} \cdot (1 - 0.40 \cdot \xi) + \nu \cdot \left(\frac{h}{d} - 0.80 \cdot \xi \right)} \quad \text{(A1)}$$

Strength ratio for anchorage failure is defined as:

$$r_\alpha = \frac{\left[\rho_{\ell,tot} \cdot \frac{\min \left\{ \frac{4 \cdot L_b \cdot f_b}{D_b} + a_{hook} \cdot 50 \cdot f_b \quad , \quad f_y \right\}}{f_c^{'}} \cdot (1 - 0.40 \cdot \xi) + \nu \cdot \left(\frac{h}{d} - 0.80 \cdot \xi \right) \right] \cdot \frac{b \cdot d^2 \cdot f_c^{'}}{h_{st}}}{\left[\rho_{\ell,tot} \cdot \frac{f_y}{f_c^{'}} \cdot (1 - 0.40 \cdot \xi) + \nu \cdot \left(\frac{h}{d} - 0.80 \cdot \xi \right) \right] \cdot \frac{b \cdot d^2 \cdot f_c^{'}}{h_{st}}} \Leftrightarrow \quad \text{(A2)}$$

$$r_\alpha = \frac{\left[\rho_{\ell,tot} \cdot \frac{\min \left\{ 4 \cdot \psi \cdot f_b + a_{hook} \cdot 50 \cdot f_b \quad , \quad f_y \right\}}{f_c^{'}} \cdot (1 - 0.40 \cdot \xi) + \nu \cdot \left(\frac{h}{d} - 0.80 \cdot \xi \right) \right]}{\left[\rho_{\ell,tot} \cdot \frac{f_y}{f_c^{'}} \cdot (1 - 0.40 \cdot \xi) + \nu \cdot \left(\frac{h}{d} - 0.80 \cdot \xi \right) \right]}$$

Strength ratio for lap splices failure is defined as:

$$r_{lap} = \frac{\left[\begin{array}{c} \min \left\{ \left(\mu_{fr} \cdot L_b \left[\frac{A_{tr}}{s} \cdot f_{st} + a_b \cdot (b - N_b \cdot D_b) \cdot f_t \right] + a_{hook} \cdot 50 \cdot N_b \cdot A_b \cdot f_b \right) \quad , \quad N_b \cdot A_b \cdot f_y \right\} \cdot \\ \cdot d \cdot (1 - 0.40 \cdot \xi) + \nu \cdot b \cdot d^2 \cdot f_c \cdot (0.50 h / d - 0.40 \cdot \xi) \end{array} \right] \Big/ (h_{st}/2)}{\left[\rho_{\ell,tot} \cdot \frac{f_y}{f_c^{'}} \cdot (1 - 0.40 \cdot \xi) + \nu \cdot \left(\frac{h}{d} - 0.80 \cdot \xi \right) \right] \cdot \frac{b \cdot d^2 \cdot f_c^{'}}{h_{st}}} \Leftrightarrow$$

$$r_{lap} \cong \frac{\min \left\{ \left(2 \cdot \psi \cdot \mu_{fr} \cdot \frac{D_b}{d} \cdot \left[\frac{A_{tr}}{b \cdot s} \cdot \frac{f_{st}}{f_c^{'}} + a_b \cdot \frac{f_t}{f_c^{'}} \right] + a_{hook} \cdot 50 \cdot \rho_{\ell,tot} \cdot \frac{f_b}{f_c^{'}} \right) \quad , \quad \rho_{\ell,tot} \cdot \frac{f_y}{f_c^{'}} \right\} \cdot (1 - 0.40 \cdot \xi) + \nu \cdot \left(\frac{h}{d} - 0.80 \cdot \xi \right)}{\left[\rho_{\ell,tot} \cdot \frac{f_y}{f_c^{'}} \cdot (1 - 0.40 \cdot \xi) + \nu \cdot \left(\frac{h}{d} - 0.80 \cdot \xi \right) \right]}$$

(A3)

Strength ratio at joint failure is defined as:

$$r_j = \frac{\gamma_j \cdot f_{ct} \cdot \sqrt{1+\frac{v_j \cdot f_c^{'}}{f_{ct}}} \cdot b_j \cdot d \cdot d_{beam}/h_{st}}{\left[\rho_{\ell,tot} \cdot \frac{f_y}{f_c^{'}} \cdot (1-0.4 \cdot \xi) + v\left(\frac{h}{d} - 0.8 \cdot \xi\right)\right] \cdot \frac{b \cdot d^2 \cdot f_c^{'}}{h_{st}}} \Leftrightarrow$$

$$r_j = \frac{\gamma_j \cdot f_{ct} \cdot \sqrt{1+\frac{v_j \cdot f_c^{'}}{f_{ct}}} \cdot b_j \cdot d \cdot d_{beam}}{\left[\rho_{\ell,tot} \cdot \frac{f_y}{f_c^{'}} \cdot (1-0.4 \cdot \xi) + v\left(\frac{h}{d} - 0.8 \cdot \xi\right)\right] \cdot b \cdot d^2 \cdot f_c^{'}} \quad \text{(A4)}$$

Strength ratio for failure due to punching at slab – columns connections is defined as:

$$r_{pn} = \frac{\left[0.12 \cdot \min\left\{1+\sqrt{\frac{200}{d_{sl}}}\ ,\ 2\right\} \cdot \left(100\rho_{\ell,sl} \cdot f_c^{'}\right)^{1/3} \cdot d_{sl} \cdot 0.25 u_{crit} \cdot (h+4d_{sl})\right] / h_{st}}{\left[\rho_{\ell,tot} \cdot \frac{f_y}{f_c^{'}} \cdot (1-0.40 \cdot \xi) + v\left(\frac{h}{d} - 0.80 \cdot \xi\right)\right] \cdot \frac{b \cdot d^2 \cdot f_c^{'}}{h_{st}}} \Leftrightarrow$$

$$r_{pn} = \frac{\frac{0.12}{f_c^{'}} \cdot \min\left\{1+\sqrt{\frac{200}{d_{sl}}}\ ,\ 2\right\} \cdot \left(100\rho_{\ell,sl} \cdot f_c^{'}\right)^{1/3} \cdot \frac{d_{sl}}{d} \cdot \frac{0.25 u_{crit}}{b} \cdot \left(\frac{h}{d} + 4\frac{d_{sl}}{d}\right)}{\left[\rho_{\ell,tot} \cdot \frac{f_s}{f_c^{'}} \cdot (1-0.40 \cdot \xi) + v\left(\frac{h}{d} - 0.80 \cdot \xi\right)\right]} \quad \text{(A5)}$$

Column strength ratio at beam yielding is given by:

$$r_{by} = \frac{\left(M_{beam}^{+} + M_{beam}^{-}\right) / h_{st}}{\left[\rho_{\ell,tot} \cdot \frac{f_y}{f_c^{'}} \cdot (1-0.4 \cdot \xi) + v\left(\frac{h}{d} - 0.8 \cdot \xi\right)\right] \cdot \frac{b \cdot d^2 \cdot f_c^{'}}{h_{st}}} \Leftrightarrow$$

$$r_{by} = \frac{0.85 \cdot \rho_{beam}}{\left[\rho_{\ell,tot} \cdot \frac{f_y}{f_c^{'}} \cdot (1-0.4 \cdot \xi) + v\left(\frac{h}{d} - 0.8 \cdot \xi\right)\right]} \cdot \frac{b_{beam} \cdot d_{beam}^2}{b \cdot d^2} \cdot \frac{f_y^{beam}}{f_c^{'}} \quad \text{(A6)}$$

where $\rho_{l,tot}$ is the total longitudinal reinforcement ratio of the column; L_b is the lap/anchorage length expressed in multiples of the main bar diameter ($L_b=\psi \cdot D_b$); f_b was calculated according to Model Code 2010 (2010) ($f_b=2 \cdot f_{b,o}$ for ribbed bars, where $f_{b,o}= n_1 n_4 \cdot (f_c'/20)^{0.5}$, n_1=1.80 for ribbed bars, n_4=1.20 for f_y=400 MPa and =1.0 for f_y=500 MPa. The anchorage capacity of a smooth bar hook was taken equal with that of a ribbed bar, $=50 \cdot f_b A_b$); f_c' is the concrete compressive strength; $f_t=0.70 \cdot (0.30 \cdot (f_c)^{2/3})$ is the concrete tensile strength; D_b is the diameter of longitudinal reinforcing bars; f_y is the longitudinal reinforcement yield stress; f_{st} is the stirrup yield stress; ξ is the normalized depth of compression zone; v_j is the axial load ratio of the column above the joint, h is the column height; d is the column depth; b is the column width; h_{st} is the deformable length of the column (equal to free storey height or to the column length in the case of captive columns); μ_{fr} is the friction coefficient ($0.2 \leq \mu fr \leq 0.3$ for smooth bars, $1 \leq \mu_{fr} \leq 1.5$ for ribbed bars); a_b is a binary index (1 or 0) depending on whether ribbed or smooth reinforcement has been used (this variable regulates the contribution of the concrete cover); a_{hook} is a binary index (1 or 0) to account for hooked anchorages (a_{hook} =0 => no hooks); N_b is the number of tension bars; A_b is the area of a single tension bar; A_{tr} is the area of stirrup legs in a single stirrup pattern in direction normal to the splitting plane; s is the

stirrup spacing; γ_j equals to 1.60 for interior joints, 1.00 for exterior joints and 0.60 for corner joints (as per ACI-ASCE 352 [13]); b_j is the joint width; d_{beam} is the beam depth; $\rho_{j,horiz}$ is the area ratio of joint horizontal reinforcement (=total area of stirrup legs in the joint parallel to the plane of action, divided by $b_j \cdot d_{beam}$); $\rho_{l,sl}$ is the total slab reinforcement ratio, at the critical punching perimeter; d_{sl} is the slab depth; u_{crit} is the critical punching perimeter around the typical column in flat plate construction. Term ρ_{beam} in A(6) refers to the total longitudinal reinforcement ratio of the beam section adjacent to the column if an interior connection is considered; in exterior connections this variable assumes the value of the top or bottom beam reinforcement ratio (whichever is largest, since the numerator in the original form of A(6) is simplified to *abs* $\max\{M_{beam}^{+}; M_{beam}^{-}\}$.).

APPENDIX B:

Storey I.D. / Column I.D.		1st	2nd	3rd	4th	5th	
C1	b×h (m)	0.31×0.32	0.30×0.30	0.28×0.28	0.25×0.25	0.25×0.25	0.
	Long.reinf.(mm)	4Ø16	4Ø16	4Ø14	4Ø14	4Ø14	
C2	b×h (m)	0.39×0.39	0.37×0.37	0.35×0.35	0.32×0.32	0.27×0.27	0.
	Long.reinf.(mm)	4Ø18	4Ø18	4Ø18	4Ø16	4Ø14	
C3	b×h (m)	0.39×0.39	0.36×0.37	0.35×0.35	0.32×0.32	0.28×0.28	0.
	Long.reinf. (mm)	4Ø18	4Ø18	4Ø18	4Ø16	4Ø14	
C4	b×h (m)	0.39×0.40	0.37×0.37	0.35×0.36	0.32×0.33	0.29×0.29	0.
	Long.reinf.(mm)	4Ø18	2Ø18+2Ø20	4Ø18	4Ø16	2Ø14+2Ø16	
C5	b×h (m)	0.39×0.40	0.37×0.38	0.36×0.36	0.33×0.34	0.29×0.29	0.
	Long.reinf.(mm)	2Ø18+2Ø20	2Ø18+2Ø20	4Ø18	4Ø16	2Ø14+2Ø16	
C6	b×h (m)	0.46×0.46	0.43×0.44	0.41×0.42	0.38×0.38	0.34×0.34	0.
	Long.reinf.(mm)	4Ø16+2Ø18	6Ø18	4Ø18+2Ø16	2Ø18+2Ø20	2Ø16+2Ø18	2Ø
C7	b×h (m)	0.43×0.43	0.41×0.41	0.39×0.39	0.36×0.36	0.31×0.32	0.
	Long.reinf.(mm)	6Ø16	4Ø16+2Ø18	6Ø16	4Ø18	4Ø16	
C8	b×h (m)	0.50×0.50	0.48×0.48	0.46×0.46	0.42×0.42	0.37×0.38	0.
	Long.reinf.(mm)	4Ø18+2Ø20	6Ø20	4Ø18+2Ø20	4Ø18+2Ø16	4Ø16+2Ø14	
C9	b×h (m)	0.30×0.30	0.29×0.29	0.28×0.27	0.25×0.25	0.25×0.25	0.
	Long.reinf.(mm)	4Ø16	2Ø14+2Ø16	4Ø14	4Ø14	4Ø14	
C10	b×h (m)	0.40×0.42	0.38×0.38	0.36×0.37	0.34×0.34	0.29×0.29	0.
	Long.reinf.(mm)	4Ø16+2Ø14	6Ø16	4Ø18	2Ø16+2Ø18	2Ø14+2Ø16	
C11	b×h (m)	0.30×0.30	0.29×0.29	0.27×0.27	0.25×0.25	0.25×0.25	0.
	Long.reinf.(mm)	4Ø16	2Ø14+2Ø16	4Ø14	4Ø14	4Ø14	
C12	b×h (m)	0.36×0.36	0.34×0.34	0.32×0.32	0.29×0.30	0.26×0.26	0.
	Long.reinf.(mm)	4Ø16	4Ø16	4Ø16	2Ø16+2Ø14	4Ø14	
C13	b×h (m)	0.60×0.41	0.58×0.38	0.55×0.36	0.53×0.31	0.48×0.27	0.
	Long.reinf.(mm)	4Ø18+2Ø20	4Ø18+2Ø20	6Ø18	6Ø16	4Ø18	

Table B: Columns cross section dimensions and longitudinal reinforcement per storey of the bu